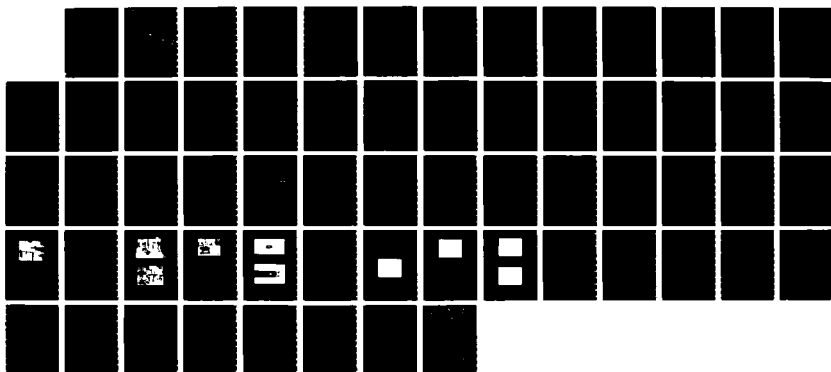ANGULAR DISTRIBUTION OF TRANSITION RADIATION IN THE
SOFT X-RAY SPECTRUM(U) NAVAL POSTGRADUATE SCHOOL
MONTEREY CA C H YIM 18 DEC 86

AD-A178 859
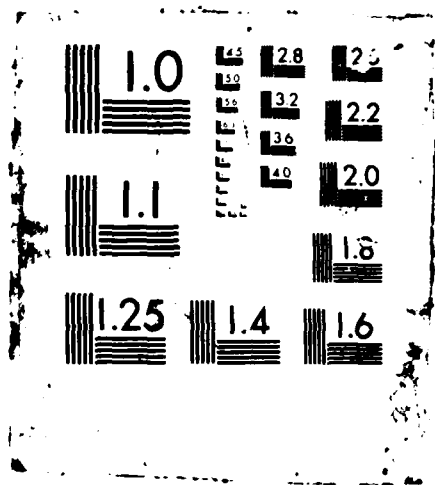
NAVAL POSTGRADUATE SCHOOL
Monterey, California

DTIC
ELECTE
APR 8 1987
S
A
D

THESIS

ANGULAR DISTRIBUTION OF TRANSITION
RADIATION
IN THE SOFT X-RAY SPECTRUM

by

Yim, Chang-Ho

December 1986

Thesis Advisor   John R. Neighbours

87   4 7 141

REPORT DOCUMENTATION PAGE

1a REPORT SECURITY CLASSIFICATION	1b RESTRICTIVE MARKINGS
UNCLASSIFIED	

2a SECURITY CLASSIFICATION AUTHORITY	3 DISTRIBUTION/AVAILABILITY OF REPORT
	Approved for public release;
2b DECLASSIFICATION/DOWNGRADING SCHEDULE	distribution is unlimited

4 PERFORMING ORGANIZATION REPORT NUMBER(S)	5 MONITORING ORGANIZATION REPORT NUMBER(S)

6a NAME OF PERFORMING ORGANIZATION	6b OFFICE SYMBOL (If applicable)	7a NAME OF MONITORING ORGANIZATION
Naval Postgraduate School	61	Naval Postgraduate School

6c ADDRESS (City, State, and ZIP Code)	7b ADDRESS (City, State, and ZIP Code)
Monterey, California 93943 - 5100	Monterey, California 93943 - 5100

8a NAME OF FUNDING/SPONSORING ORGANIZATION	8b OFFICE SYMBOL (If applicable)	9 PROCUREMENT INSTRUMENT IDENTIFICATION NUMBER

8c ADDRESS (City, State, and ZIP Code)	10 SOURCE OF FUNDING NUMBERS			
	PROGRAM ELEMENT NO	PROJECT NO	TASK NO	WORK UNIT ACCESSION NO

11 TITLE (Include Security Classification)

Angular Distribution of Transition Radiation in the Soft X-Ray Spectrum

12 PERSONAL AUTHOR(S) Yim, Chang-Ho

13a TYPE OF REPORT	13b TIME COVERED	14 DATE OF REPORT (Year, Month, Day)	15 PAGE COUNT
Master's Thesis	FROM _____ TO _____	1990, 12, 12	62

16 SUPPLEMENTARY NOTATION

17	COSATI CODES		18 SUBJECT TERMS (Continue on reverse if necessary and identify by block number)
FIELD	GROUP	SUB-GROUP	Emission angle; Angular distribution; Transition radiation;
			Soft x-ray; Interference; Multifoil stack; Radiation cone.

19 ABSTRACT (Continue on reverse if necessary and identify by block number)

The angular distribution of transition radiation has been investigated theoretically and experimentally. The theoretical prediction and the computer graphic analysis are presented in families of plots which illustrate the dependence of the intensity on the emission angle. Although the experimental method used had limited resolution, the optimum cone angles of the x-ray radiation were in agreement with the theoretical values. Problems encountered during the experiment are discussed for continuing work. This work may have several important applications in electron beam diagnostics. These include monitoring of the beam emittance and energy. Keywords; ....

20 DISTRIBUTION/AVAILABILITY OF ABSTRACT	21 ABSTRACT SECURITY CLASSIFICATION	
☒ UNCLASSIFIED/UNLIMITED ☐ SAME AS RPT ☐ DTIC USERS	Unclassified	

22a NAME OF RESPONSIBLE INDIVIDUAL	22b TELEPHONE (Include Area Code)	22c OFFICE SYMBOL
Professor John P. Neighbours	(408) 646 - 2922	61nb

DD FORM 1473, 84 MAR	83 APR edition may be used until exhausted	SECURITY CLASSIFICATION OF THIS PAGE
	All other editions are obsolete	

Angular Distribution of Transition Radiation
in the Soft X-Ray Spectrum

by

Yim, Chang-Ho
Major, Republic of Korea Army
B.S., R.O.K. Military Academy, 1975

Submitted in partial fulfillment of the
requirements for the degree of

MASTER OF SCIENCE IN PHYSICS

from the
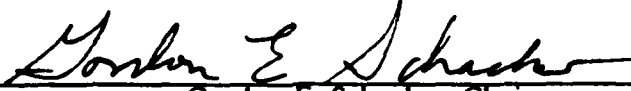
NAVAL POSTGRADUATE SCHOOL
December 1986

Author: _____
Yim, Chang-Ho

Approved by: _____
John R. Neighbours, Thesis Advisor

_____
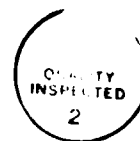Fred R. Buskirk, Second Reader

_____
Gordon E. Schacher, Chairman,
Department of Physics

_____
John. N. Dyer,
Dean of Science and Engineering

2

ABSTRACT

The angular distribution of transition radiation has been investigated theoretically and experimentally. The theoretical prediction and the computer graphic analysis are presented in families of plots which illustrate the dependence of the intensity on the emission angle. Although the experimental method used had limited resolution, the optimum cone angles of the x-ray radiation were in agreement with the theoretical values. Problems encountered during the experiment are discussed for continuing work. This work may have several important applications in electron beam diagnostics. These include monitoring of the beam emittance and energy.

3

TABLE OF CONTENTS

LIST OF TABLES

LIST OF FIGURES

7

ACKNOWLEDGEMENTS

I am grateful to my thesis advisor, Professor John R. Neighbours and my second reader, Professor Fred R. Buskirk, for their guidance and instructions in completing this thesis work.

Special thanks are due to Dr. M. A. Piestrup, who is a Senior Research Associate in the Department of Electrical Engineering, Stanford University in the field of free-electron lasers and the president of Adelphi Technology, initiated the experiment and gave helpful comments.

I also would like to acknowledge the support by Mr. Don Snyder who gave all the assistances for my experimental work concerned with LINAC.

A very special thanks to my wife and children, Young-Ja, Do-Ran and Hong-Jae, for their typing, editing this thesis and being patient for two and half years in the United States of America.

I. INTRODUCTION

A. HISTORY

While theoreticians in the USSR intensively studied Cerenkov radiation [Ref. 1], V. L. Ginsburg and I. M. Frank observed a radiation produced with a continuous spectrum stretching from the longest wave to ultraviolet waves when a uniformly moving charged particle traversed the interface of two media, in particular, from the vacuum into a metal. This radiation was described as a transition radiation and, in order to explain the nature of this phenomenon, the theory of radiation of the electron from vacuum into a perfect conductor was derived for a single interface. [Ref. 2] Although transition radiation was predicted in 1946 and investigated in extensive theoretical studies since then, it did not receive adequate attention through the years because the radiation yield produced from a single interface is very weak [Ref. 3].

In 1958, G. M. Garibyan predicted that the total transition radiation yield is proportional to the energy of the moving particle, causing interests to be renewed in the application of this property to the identification of high-energy particles and to astrophysics [Refs. 1,4: pp. 3644,1306]. Due to the low intensity of the radiation, I. M. Frank suggested the use of a stack of foils rather than a single one, and the use of such a stack became very important for the identification of high-energy particles. [Refs. 1,5: pp. 3644,1794]

After R. F. Arutyunyan and others observed x-ray transition radiation in 1962, E. S. Belyakov and others observed the interference effect of transition radiation in the hard x-ray region. But difficulty in finding the experimental evidence due to the large background level in this region delayed the study of the x-ray interference effect in transition radiation [Refs. 1,6,7].

In recent years, rather than thick foils which were used to produce hard x-rays, thin foils that produce soft x-ray transition radiation were considered [Ref. 8]. But, an impasse is reached, since as the intensity of the transition x-rays is increased by a multifoil stack, the absorption of the x-rays is also increased [Ref. 7: p. 1773]. Much work has been done in an attempt to solve the problem of a stack with some success.

B. WHAT IS TRANSITION RADIATION?

It may be seen, by the laws of conservation of energy and momentum, that a charged particle moving uniformly in a homogeneous medium does not radiate electromagnetic waves. Exceptionally an electron moving uniformly in a homogeneous medium radiates when its velocity is faster than the phase velocity of light through the same medium, as it is well known, which is Cerenkov radiation. [Ref. 3: p. 194]

In a medium the radiation depends not only on the velocity of the particle but also on the optical properties of this medium. A charged particle, moving uniformly, radiates if the properties of the medium vary along its path, that is, it radiates when crossing the boundary between two different dielectric media. [Ref. 3: p. 195]

Transition radiation is the electromagnetic radiation which is emitted when a uniformly moving charged particle traverses from one medium into another with a different dielectric constant. More generally the effect will occur in the presence of heterogeneity in a medium. [Ref. 2: p. 353] Although transition radiation can be considered as a kind of Cerenkov radiation and is closely associated with the Cerenkov effect, the generation mechanism of transition radiation is different, because transition radiation occurs for any arbitrary velocity of a charged particle while Cerenkov radiation depends primarily on the particle velocity being heigher than the velocity of light. Transition radiation, whose intensity is strongly dependent on the energy of the charged particle, is angular dependent. [Ref. 2: p. 353]

For ultra-relativistic particles, $E mc^2 = \gamma$ much greater than unity, the major part of the radiated energy is in the x-ray region, and for a single boundary the radiation yield produced by an individual electron is very weak; on the order of one photon for a hundred electrons. Therefore, a stack of foils rather than a single one is used in most practical observations of the effect. [Ref. 6]

C. MAIN CHARACTERISTICS

Transition radiation is characterized by several features:

(1) The emission angle between the photons and the moving charged particles is given by $\theta \sim 1/\gamma$. For the ordinary incoherent transition radiation with $\gamma < 10^4$, radiated photons will be well collimated with a small emission angle (see Figure 1.1). [Ref. 6: p. 3]

(2) The total integrated energy is proportional to γ. The application of this property is the main goal for high-energy particle detection. [Ref. 6: p. 9]

11

(3)   In the case of a periodic medium, an rπ phase difference is the condition for constructive interference or resonance between radiation produced at successive interfaces, where r is an positive integer .

(4)   The radiation is polarized in the plane containing the particle velocity vector and the wave propagation vector.

Cerenkov radiation has characteristics (1) and (4).

FOIL STACK

ELECTRON BEAM

The transition radiation cone is produced by a relativistic electron beam passing through a stack of multifoil. The angle of the cone, θ, depends upon the incident energy of the electron beam.
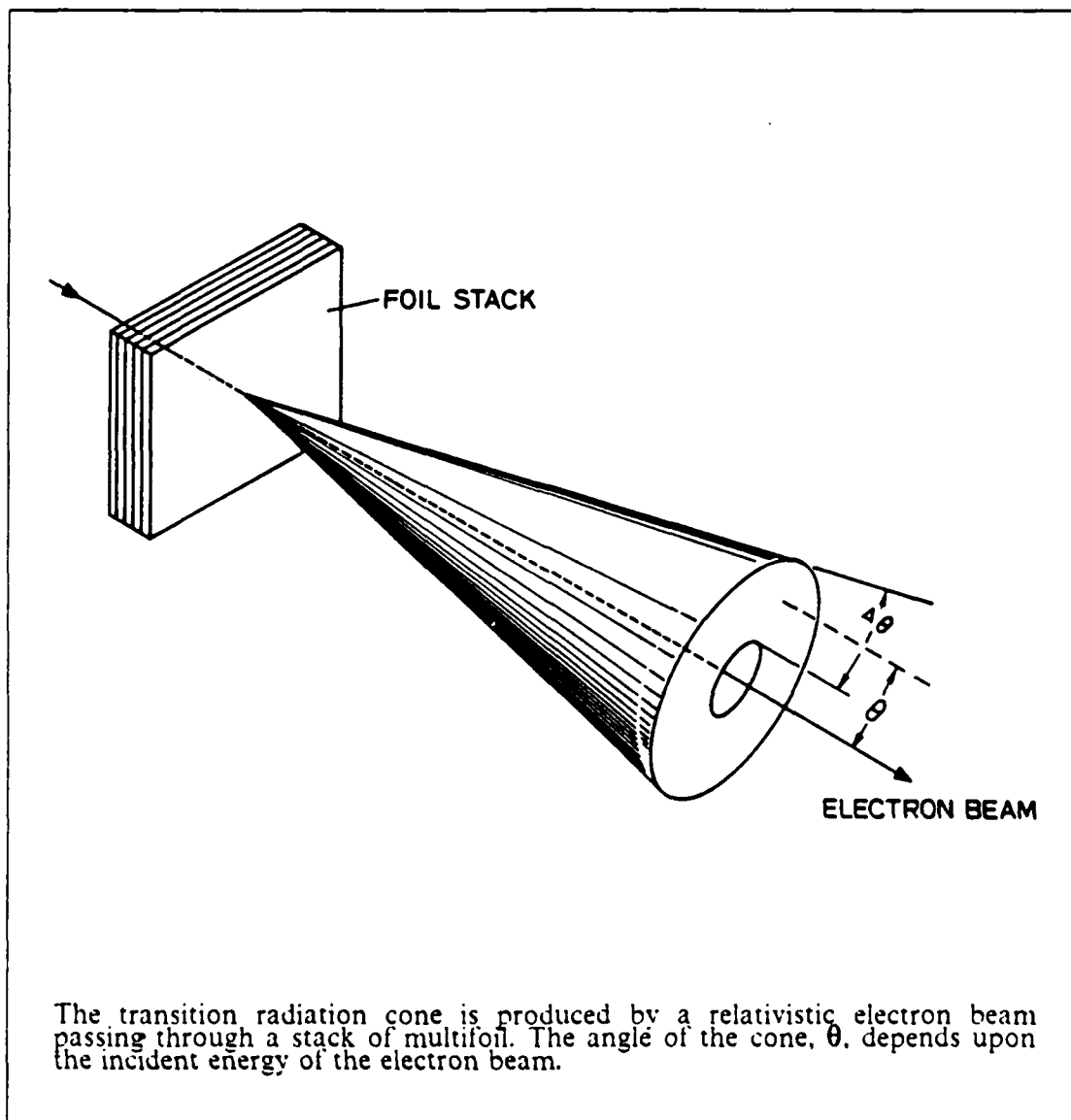
Figure 1.1   Schematic diagram of the transition radiation cone.

D. PREVIOUS EXPERIMENTS AT NPS

Only one experiment considering transition radiation has been conducted by Professor Fred R. Buskirk and others in the Naval Postgraduate school since the LINAC was established. The experiment was aimed to verify that transition radiation is a source of x-rays in the spectral range of 800eV-1000eV. Targets of Al, Be, and Mylar were used. To keep the thin foils flat without wrinkles, relatively thick spacers of stainless steel of 1.5mm thickness and aluminum of 0.51mm thickness were chosen. The foil stacks produced both transition radiation and bremsstrahlung radiation. Single foils with a thickness equivalent to M foils were used to obtain and subtract the bremsstrahlung background radiation from the transition radiation produced by the stack of multifoils. The results were that the bremsstrahlung was too high and bandwidth of the measured curves was too broad, because there was other background noise in addition to the bremsstrahlung. However the position of the peak value of the spectrum agreed with the expected one. [Ref. 7: pp. 1775-1776]

E. PURPOSE

The object of this experiment is to obtain the soft x-ray spectrum from a stack of thin foils of mylar. The spectrum is calibrated and distinguished by comparison to the spectrum of Fe^{55} which decays to Mn^{55} through the electron capture, which radiates x-ray of the peak energy 6KeV. Primary effort should be focused on noise reduction, as learned from previous work, and to scan to get the angular distribution of the radiation and the interference effect, using a much thinner spacers than those used previously.

II. THEORY

A. THEORETICAL REVIEW

The theoretical expression for the spectral intensity of transition radiation is somewhat complicated. However, in order to do this experiment, a detailed review of the fundamental derivation is not necessary. The basic formula (equation 2.1) is analyzed as a multiplied function of three different functions, for example $F(\omega,\theta)$, $F(\ell,Z)$ and $F(M,X)$.

The number of photons produced per unit frequency and per unit solid angle from a single electron crossing M foil pairs (*i.e.* 2 M interfaces), each composed of two materials of thickness ℓ_1 and ℓ_2 is given by [Refs. 4,9]:

$$\frac{d^2N}{d\Omega d\omega} = \frac{d^2N_0}{d\Omega d\omega} 4\sin^2(\frac{\ell_2}{Z_2}) \, F(M,X),$$

(2.1)

where the term

$$\frac{d^2N_0}{d\Omega d\omega} = \frac{\alpha\omega\sin^2\theta}{16\pi^2c^2} (Z_1 - Z_2)^2$$

(2.2)

describes the intensity of the radiation generated from a single interface between vacuum and a material. The $\sin^2\theta$ function and the θ dependence of $(Z_1 - Z_2)^2$ gives the shape of the radiation cone, and Z_1 and Z_2 are defined as *formation lengths* [Ref. 5] given by:

$$Z_i = \frac{2\beta c}{\omega[1 - \beta(\varepsilon_i - \sin^2\theta)^{1/2}]}.$$

(2.3)

where $\quad\beta \ : \ \upsilon c$

$\qquad\upsilon \ : \ $ the speed of electron

$\qquad c \ : \ $ the speed of light in a medium

$\qquad i \ : \ 1,2$

$\qquad\varepsilon_i = 1 - (\omega_i \omega)^2 \ : \ $ the permittivity of the dielectric medium

14

ω_i : the plasma frequency

ω : the photon frequency

α : the fine structure constant (approximately $1/137$)

$\gamma = 1/(1 - \beta^2)^{1/2}$

: the ratio of the electron energy to its rest energy (E/E_0)

in MKS units. The parameter X is given by:

$$X = \frac{\ell_1}{Z_1} + \frac{\ell_2}{Z_2}. \tag{2.4}$$

Using the small angle approximation $\sin\theta \sim \theta$ and $\beta \sim 1 - 1/2\gamma^2$ by binomial expansion, equation 2.3 can be easily transformed to:

$$Z_i = \frac{4\lambda'}{(1/\gamma)^2 + \theta^2 + (\omega_i/\omega)^2}, \tag{2.5}$$

which agrees with the equation given by M. L. Cherry in [Ref. 5], where $\lambda' = c/\omega$.

Substituting equation 2.5 into the equation 2.2 and differentiating with respect to θ (where $\sin\theta \sim \theta$), the optimizing angle of the cone where transition radiation from an electron crossing a single interface is most intense is derived to be [Ref. 9: p. 1290]:

$$\theta^2_{opt} \sim \frac{1}{3} \{[(\delta_1 + \delta_2)^2 + 12\delta_1\delta_2]^{1/2} - (\delta_1 + \delta_2)\}, \tag{2.6}$$

where $\delta_i = [(1/\gamma)^2 + (\omega_i/\omega)^2]/2$ with $i = 1, 2$. For the case of a foil stack in vacuum, $\omega_1 = 0$, equation 2.6 becomes (see Figure 1.1 and 2.1):

$$\theta_{opt} \sim 1/\gamma. \tag{2.7}$$

The second term of equation 2.1 , $4\sin^2(\ell_2/Z_2)$, accounts for coherent addition of amplitudes from the two interfaces of a single foil. This term contributes to the maximum intensity when $\sin^2(\ell_2/Z_2) = 1$.

The radiation is radiated in a small cone of half angle $\theta = 1/\gamma$ with respect to the direction of the moving electron beam. The figure shows how the coherent radiation differs from the incoherent radiation. For an electron energy 65MeV, $\theta \sim \Delta \theta \sim 1/\gamma = 7.9$mrad.
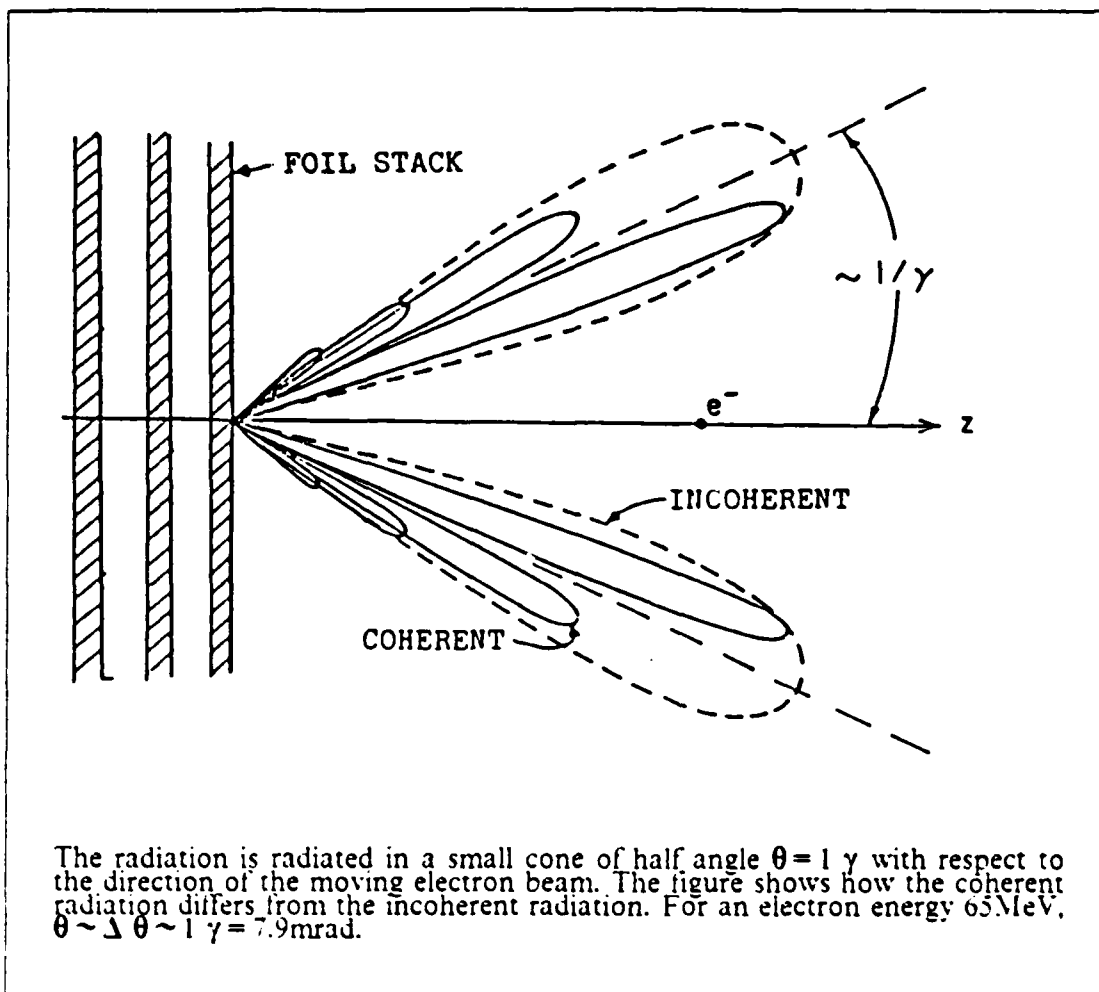
Figure 2.1   Transition radiation from a foil stack.

From equation 2.1 which is the differential efficiency. the factor taking into account interference between radiation from successive foils is given by [Ref. 9]:

$$F(M,X) = \frac{1 + \exp(-M\sigma) - 2\exp(-M\sigma/2)\cos(2MX)}{1 + \exp(-\sigma) - 2\exp(-\sigma/2)\cos(2X)}. \tag{2.8}$$

with $\sigma = \mu_1 \ell_1 + \mu_2 \ell_2$, where $\mu_{1,2}$ is the absorption coefficient of medium 1, 2 (for vacuum spacing, $\mu_1 = 0$).

At high photon energies. x-ray absorption becomes negligible. In this case equation 2.8 becomes:

16

$$F(M,X) \sim \frac{\sin^2(MX)}{\sin^2(X)}. \tag{2.9}$$

So that the multi-foil expression, equation 2.1 reduces to that derived by G. M. Garibyan: [Ref. 4]

$$\frac{d^2N}{d\Omega d\omega} = \frac{d^2N_0}{d\Omega d\omega} 4\sin^2(\frac{\ell_2}{Z_2})(\frac{\sin MX}{\sin X})^2. \tag{2.10}$$

This figures are the theoretical transition radiation patterns for the two foil stack with the spacing of 0.003″, the foil thickness of 2.5μm, and γ = 127.
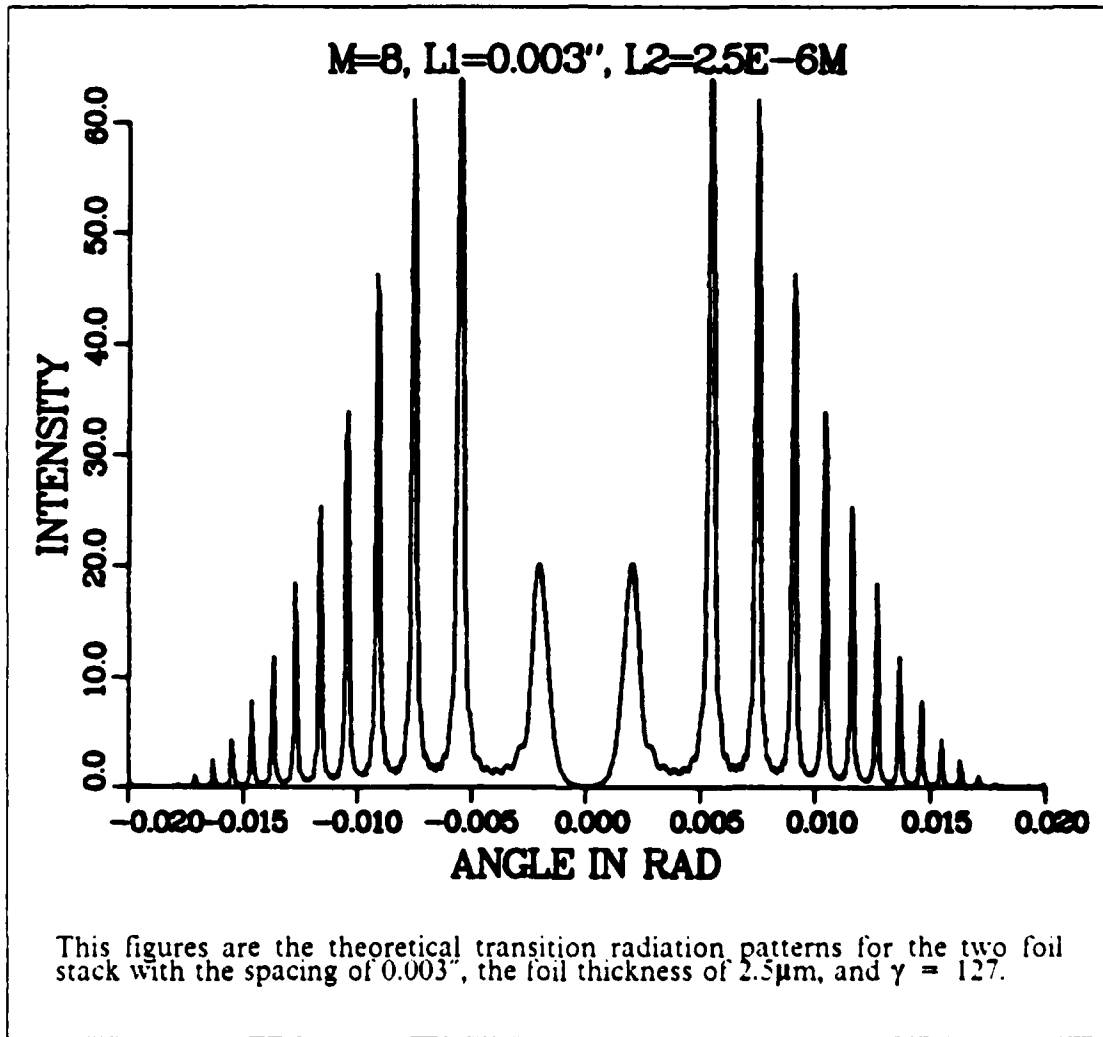
Figure 2.2   Theoretical coherent transition radiation.

17

In this formulation, the more rapid variation of the intensity is indicated by the third term, $[(\sin MX)(\sin X)]^2$, considered as a interference term. A simple inspection of that term shows that as M increases, the bandwidth of the maxima becomes smaller and more defined. That is, the curve of the angular distribution varies much more rapidly compared with the single interface term as shown in Figure 2.3. The principle maxima of equation 2.9 occur when:

$$X = r\pi, \tag{2.11}$$

where r is positive integer. Further information is shown in Table 1.

TABLE 1

INTERFERENCE EFFECT FOR VARIOUS X

	X =			
principle maxima	0	π	2π	3π
2nd maxima	$\dfrac{1\pi}{2M}$	$\dfrac{3\pi}{2M}$	$\dfrac{5\pi}{2M}$	$\dfrac{7\pi}{2M}$
minima (or zeros)	$\dfrac{\pi}{M}$	$\dfrac{2\pi}{M}$	$\dfrac{3\pi}{M}$	$\dfrac{4\pi}{M}$

The value of **sinMX/sinX** at a maximum is inspected as:

$$\lim_{X \to r\pi} \left(\frac{\sin MX}{\sin X}\right) = \frac{0}{0}. \tag{2.12}$$

Equation 2.12, since it is undefined by using L'Hopital's rule, can be written by:

$$\lim_{X \to r\pi} \frac{M\cos MX}{\cos X} = M, \tag{2.13}$$

18

where r is integer. Hence the intensity (*i.e.* relative photon number) at maxima increases as M^2, that is:

$$\frac{d^2N}{d\Omega d\omega} \propto M^2. \tag{2.14}$$

For a periodic stack of dielectrics, the foil thickness at which the maximum photon production occurs can be easily calculated. As seen above, the maximum photon production occurs for $X = r\pi$, substituting for X from equation 2.4 gives:

$$X = \frac{\ell_1}{Z_1} + \frac{\ell_2}{Z_2} = r\pi. \tag{2.15}$$

Also, a single foil interference term, $\sin^2(\ell_2/Z_2)$, contributes to the maximum photon production for:

$$\frac{\ell_2}{Z_2} = (m - \frac{1}{2})\pi, \tag{2.16}$$

or:

$$\ell_2 = (m - \frac{1}{2})\pi Z_2, \tag{2.17}$$

$$\ell_1 = (r - m + \frac{1}{2})\pi Z_1, \tag{2.18}$$

where r and m are positive integers ($m \leq r$). Thus, there is emission at the interface if the material thickness of both sides of the interface is of the order of Z_1 and Z_2, or of the order of Z_2 in a vacuum with spacing of the order of Z_1.
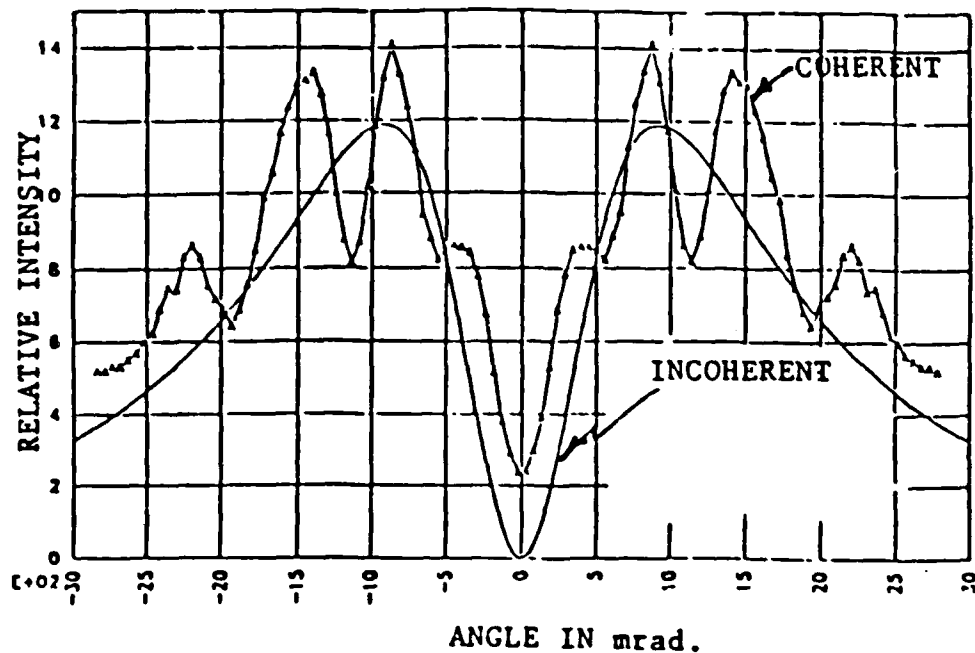
Figure 2.3 Comparison of angular distribution of coherent and incoherent radiation..

For an ultrarelativistic electron beam. the formation length Z_1. the vacuum spacing. is simplified to:

$$Z_1 \sim \frac{4\lambda}{1/\gamma^2 + (\omega_1/\omega)^2 - \theta^2}$$

(2.19)

or when $\omega_1 = 0$

$$Z_1 \sim 2\gamma^2\lambda.$$

(2.20)

where $\omega_1 = 0$ for vacuum.

Equation 2.18 is a critical requirement for vacuum spacing for $\ell_1 \geq Z_1$, therefore:

$$\ell_1 \geq 2\gamma^2\lambda'. \tag{2.21}$$

This figure shows the theoretical x-ray production from stacks of various thickness of foils. Mylar stacks of 25 foils is used. Beam energy is 100 MeV, the separation is 0.51mm. As the thickness varies, the peak of the radiation varies in amplitude and in position [Ref. 9].
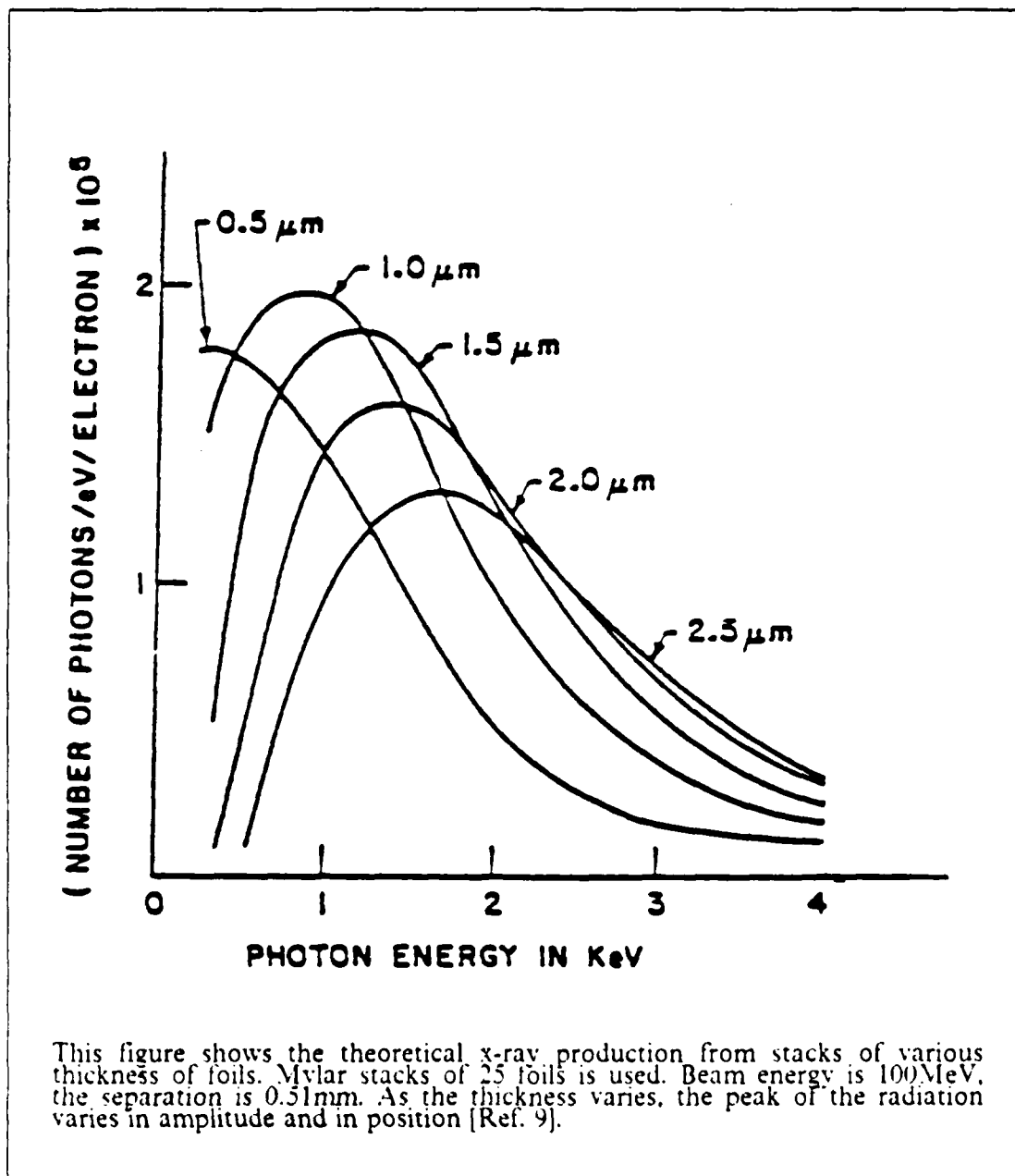
Figure 2.4 Theoretically predicted spectrum.

From equation 2.10 and 2.17, $\sin^2(\ell_2 Z_2) = 1$, the phase difference is $\pi 2$. Whereupon equation 2.10 becomes:

$$\frac{d^2 N}{d\Omega d\omega} = \frac{d^2 N_0}{d\Omega d\omega} \, 4 \left(\frac{\sin MX}{\sin X} \right)^2. \tag{2.22}$$

Comparing equation 2.22 to equation 2.14 gives:

$$\frac{d^2 N}{d\Omega d\omega} = 4M^2 \frac{d^2 N_0}{d\Omega d\omega}. \tag{2.23}$$

Thus, by selecting the foil thickness to be given by equation 2.17 and equation 2.18, it is seen that the peak of the spectral intensity varies as the square of the number of interfaces, that is:

$$\frac{d^2 N}{d\Omega d\omega} \propto (2M)^2 \tag{2.24}$$

On the other hand, when the losses by absorption of the foils are considered, the average value of equation 2.8 is given by [Ref. 10]:

$$< F(M,X) > \; = \; \frac{1 - \exp(-M\sigma)}{\sigma}, \tag{2.25}$$

and taking differentiating with respect to M and taking the first two terms of the exponential series gives $M \sim 2 \sigma$, since $\mu_1 = 0$ for the vacuum. The number of foils can be chosen by:

$$M \leq 2 \, \mu_2 \ell_2. \tag{2.26}$$

For the in-phase addition, the change of electron direction by scattering should be less than the radiation cone without scattering. The angular width without scattering is given by [Ref. 9: p. 1291]:

$$\Delta \theta_d \sim \frac{1}{M} \left(\frac{2\lambda}{\ell_1 + \ell_2} \right)^{1/2}, \tag{2.27}$$

where λ is the wavelength of the radiation.

From condition equation 2.24, the peak of the intensity structure added by the interference is proportional to the square of the number of interfaces, while the spectral and angular bandwidths are inversely proportional to the number of foils. Also the angular bandwidth depends on the foil thickness, the spacing distance and the wavelength of radiation. For the given foil thickness, the wavelength and the number of foils, the angular bandwidth increases as the separation decreased. That is why the delicate thin spacers are used in this experiment.

B.   GRAPHIC ANALYSIS BY COMPUTER

For the purpose of analysis of the expression for the x-ray radiation intensity (equation 2.1) many approximations have been made as seen in the previous section which is the mathematical summary.

In this section, computer graphics are used to make the differential form of intensity of the x-ray radiation for a periodic radiation of M foils with the thickness ℓ_2 and the spacing ℓ_1 visual by using as few approximations as possible. An example computer program in FORTRAN language is introduced in Appendix A. In most case, the same parameters as they are used in the experiment are used to get as many predictions as possible, concentrating on the angular distribution.

1. Formation Length

Physically, the formation length, in a given medium between particle and radiated photon, is of the order of the photon wavelength. The transition radiation intensity depends on the formation length as follows:

(a)   The intensity of the single interface (the first term of equation 2.1) depends on $(Z_1 - Z_2)^2$.

(b)   The single foil interference (the second term of equation 2.1)depends on $\ell_2 Z_2$.

(c)   The multi-foil interference (the third term of equation 2.1) depends on $X = \ell_1 Z_1 + \ell_2 Z_2$.

The formation length is the function of γ, the emission angle, the plasma frequency and the radiation frequency.

23
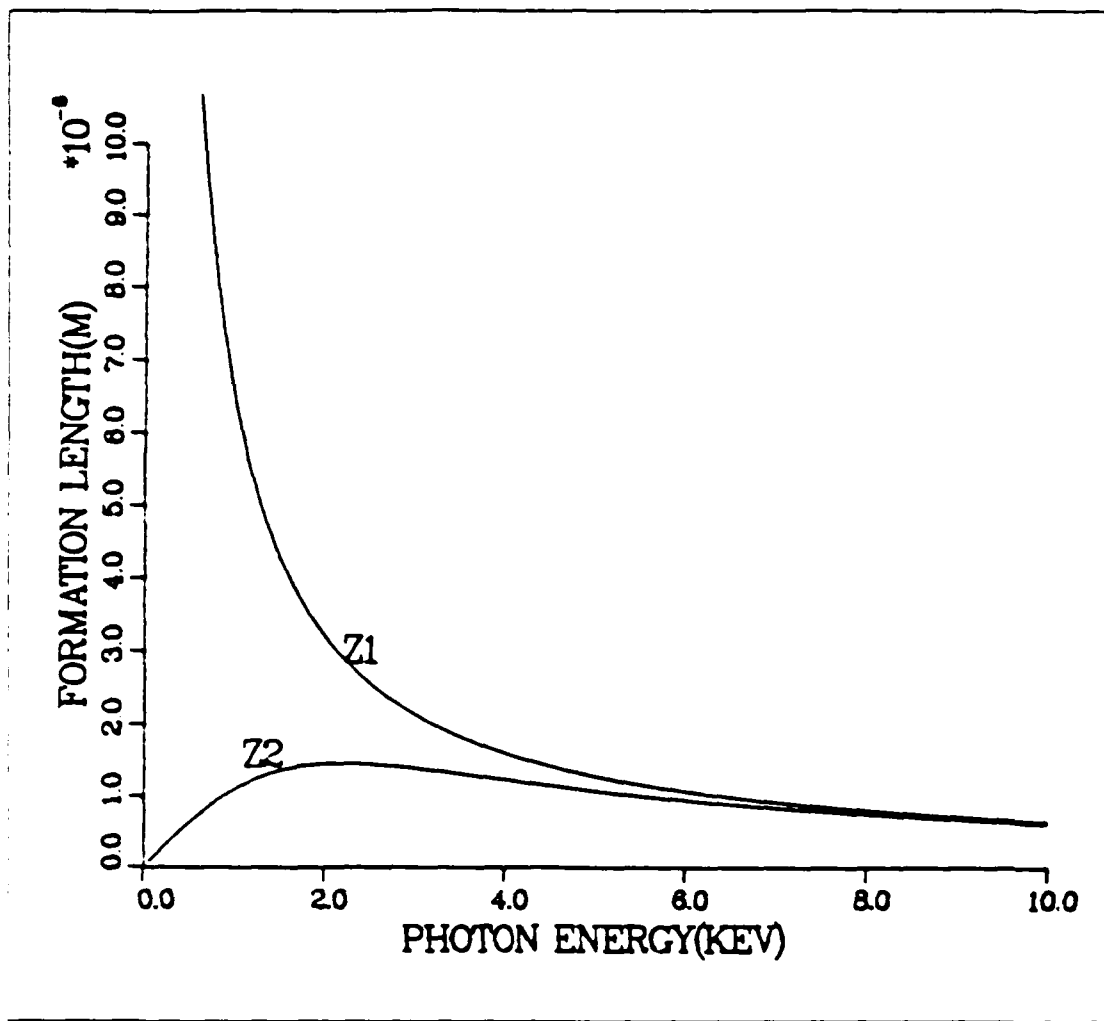
Figure 2.5　The dependence of the formation length of vacuum spacing and mylar on the emission angle.

Figure 2.5 shows the dependence of the formation length of vacuum ($\omega_1 = 0$) and mylar ($E_2 = 24.4eV$) on emission angle for a photon energy $E = 1.2keV$ which is an arbitrary value and $\gamma = 12^7$. As seen in Figure 2.5, the formation length is inversely proportional to the square of emission angle, that is why the formation length Z has a maximum value at $\theta = 0$ in the angular distribution. For comparison, the dependence of the formation length on the photon energy is shown in Figure 2.6. Figure 2.7 shows the dependence of the formation length on plasma energies of mylar ($E_2 = 24.4eV$) and Aluminum ($E_2 = 15.8eV$) for $E = 1.2 keV$ and $\gamma = 12^7$.

24
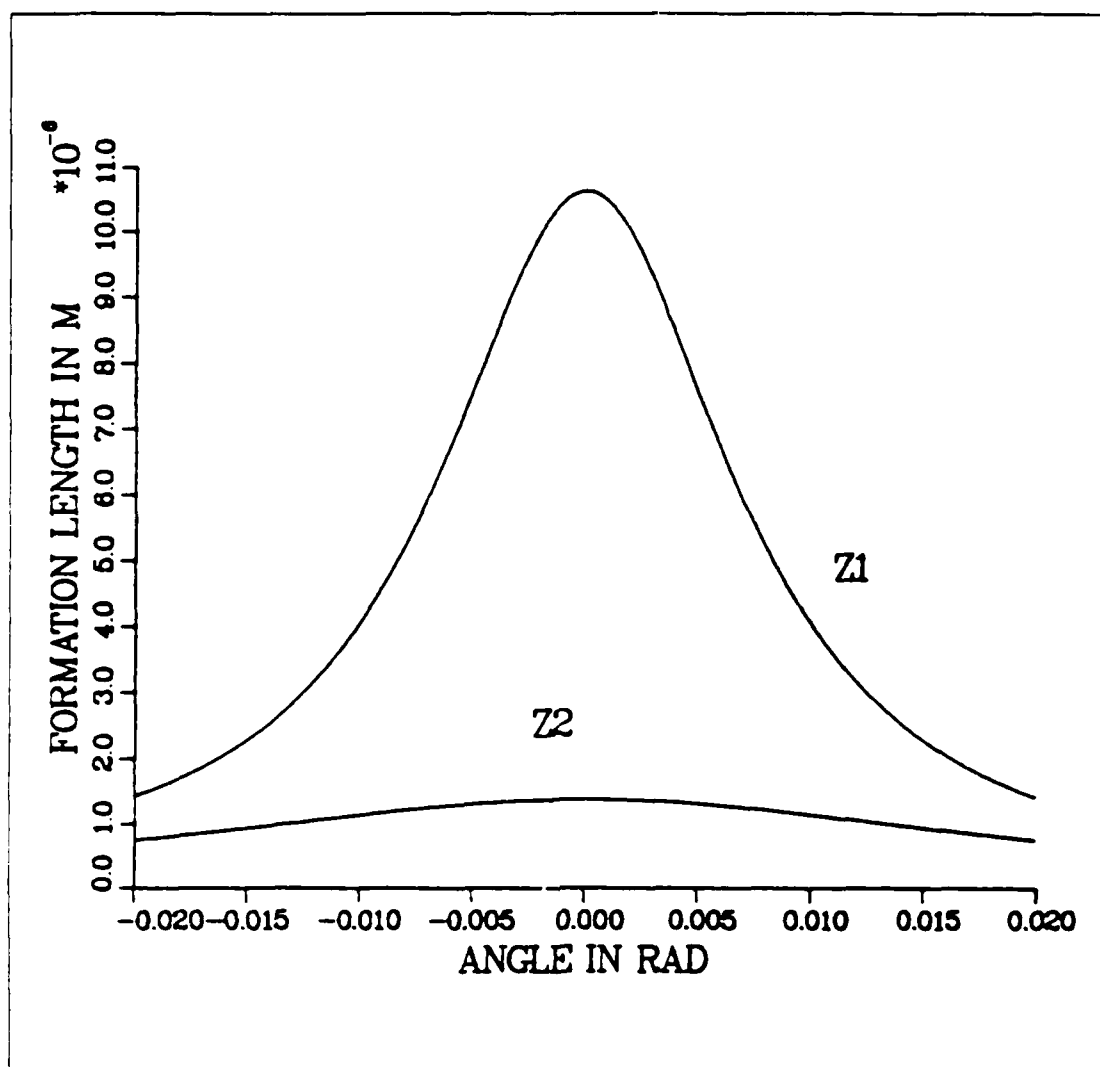
Figure 2.6   The dependence of the formation length of vacuum spacing and mylar foil on the photon energy.

2. Single Interface

The first part of the equation 2.1 is due to the intensity of the single interface radiation. The transition radiation generated at a single interface can not be observed experimentally. In practice, the particle passes at least two interfaces. But this term can be used to analyze as a typical transition radiation yield. Figures 2.8 and 2.9 show the angular distribution of the x-ray intensity produced from the single interface, which is contributed by the term $(\alpha\omega\ \sin^2\theta \cdot 16\pi^2 c^2)(Z_1 - Z_2)^2$.
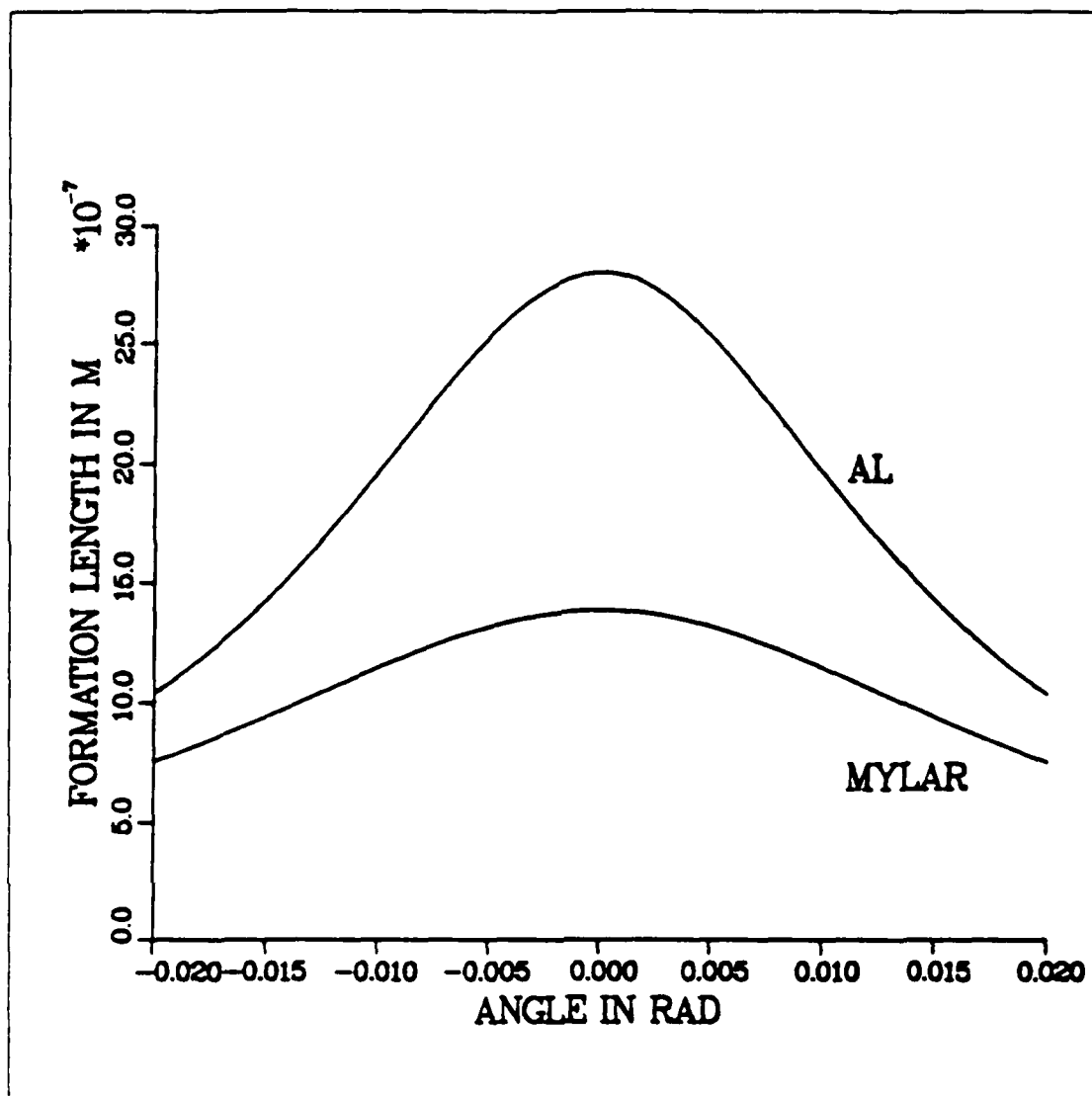
Figure 2.7   Angular distribution of the formation length of the foil with the different plasma energies.

As seen in Figure 2.8, the relative intensity is higher and more directional for the higher energy. For this Figure, $E = 1.2$ keV and $E_2 = 24.4$ eV are used. The peaks of the radiation cone can be calculated from equation 2.6 or equation 2.7. However, the practical angular peaks differs somewhat from the calculated θ_{opt}, since equations 2.6 and 2.7 are derived only for the single interface which does not depend on the foil thickness.

This figure is obtained from the first term of equation 2.1 with E_2 = 24.4 for mylar, γ = 127 where E_2 = $\hbar\omega_2$.
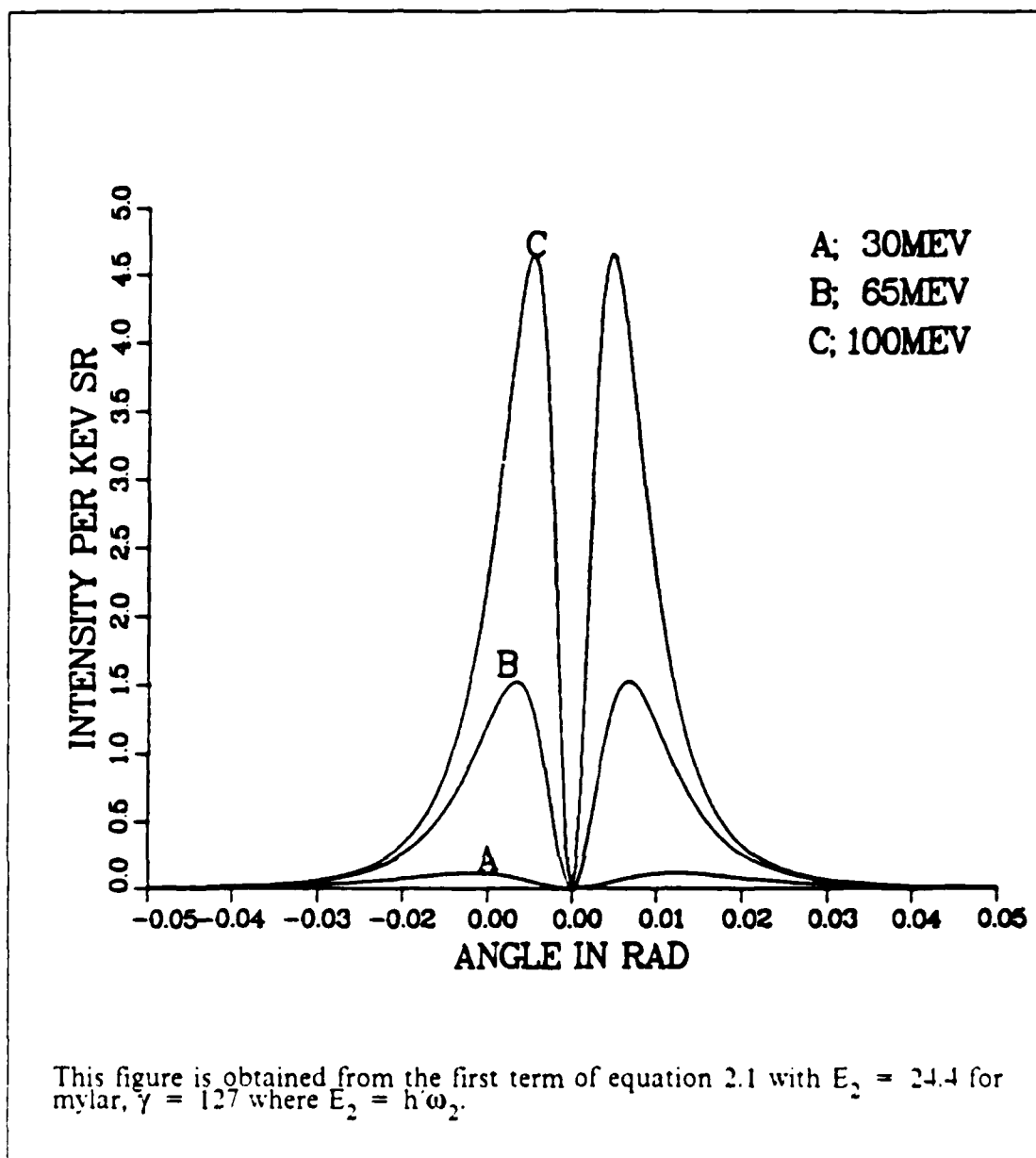
Figure 2.8   Angular distribution of photon production of the single interface with the different beam energies.

Figure 2.9 compares the difference in the angular distribution depending on the plasma frequency (24.4eV for mylar, 15.8eV for aluminum). As the plasma frequency of the medium increases, the peak angle of the radiation cone decreases and the intensity of the radiation becomes brighter.

27
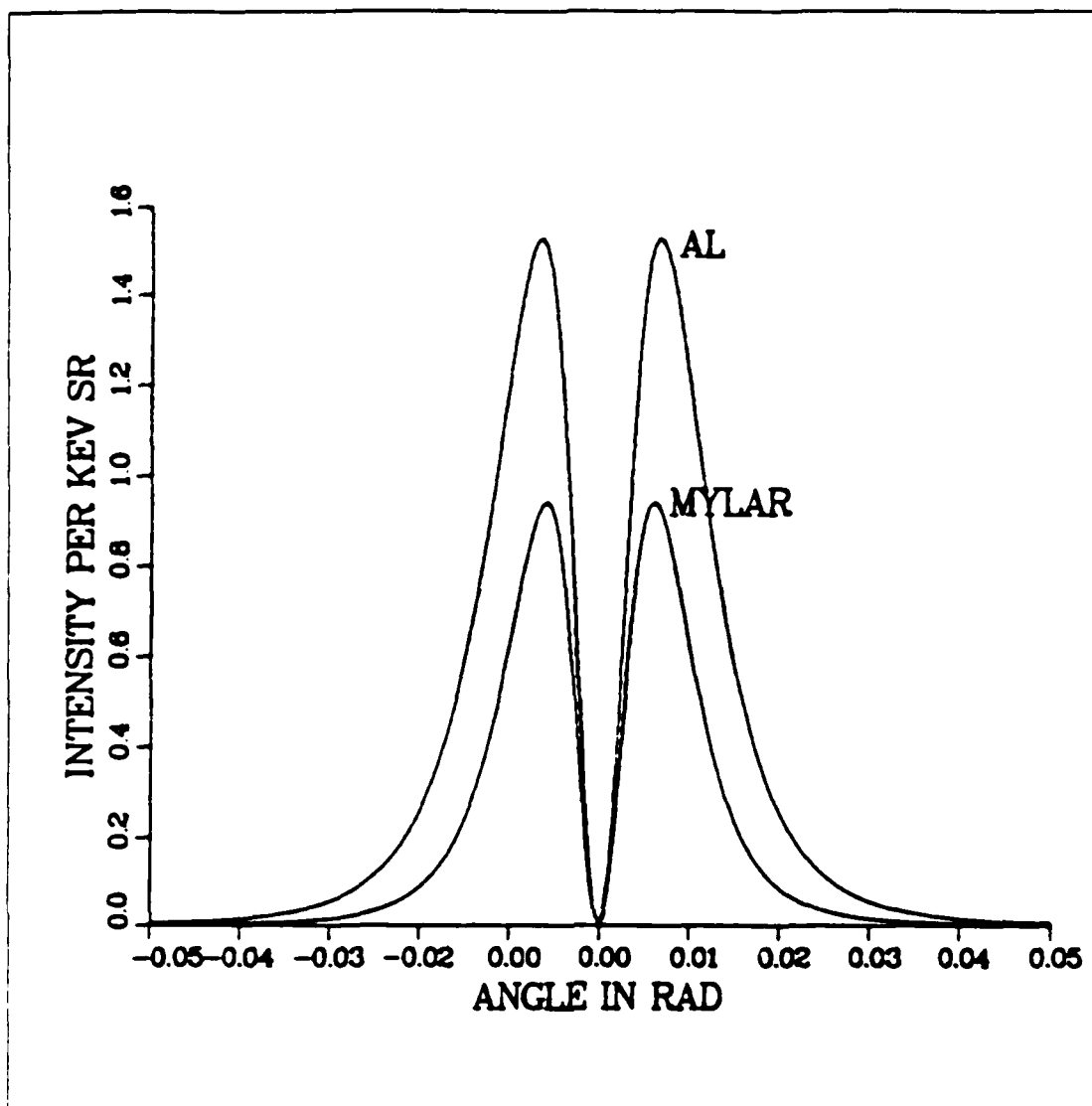
Figure 2.9   Angular distribution of photon production of the single interface
with the different plasma frequencies.

3. Single Foil Interference

The second term $\sin^2(\ell_2 Z_2)$ in equation 2.1 represents the interference of a single foil with the thickness of ℓ_2 and oscillates rapidly as compared to the range in which the first term of equation 2.1 varies as shown in Figure 2.10. The oscillation is more rapid for the range of foil thickness that is much greater than the formation length of the foil, $\ell_2 >> Z_2$.
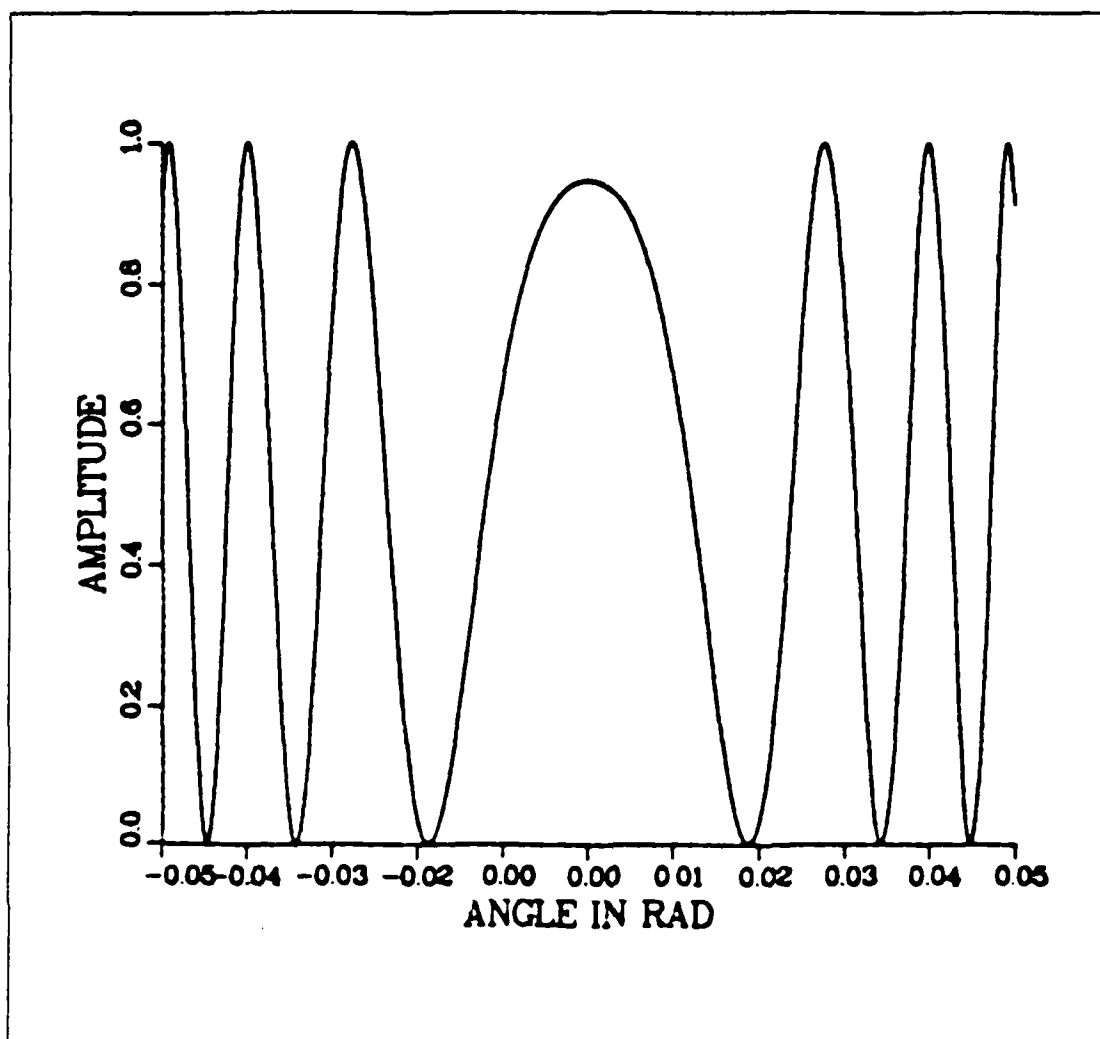
Figure 2.10 Angular distribution of the interference effect of a single foil.

4. Multifoil Interference

Multifoil interference is represented by the third term of equation 2.1. This term behaves like a pure interference term if the absorption of the medium is negligible as shown in Figure 2.11. In fact, the absorption is negligible only for the high photon energy. The absorption of the medium can not be neglected in the soft x-ray range; so equation 2.8 is considered as it is, where $\sigma = \mu_1 \ell_2 + \mu_2 \ell_2$. To see the apparent difference, the frequency distribution of the multi-foil interference effect is shown in Figure 2.12.

29

INTERFERENCE (ASSUME NO ABSORPTION)
M=8, L1=0.003", L2=2.5E-6M

INTERFERENCE AND ABSORPTION FACTOR
M=8, L1=0.003", L2=2.5E-6M

The parameters of the 8-mylar foil stack are used with the thickness of 2.5μm, the vacuum spacing of 0.003", and γ = 12⁷ in this figure.

Figure 2.11   Angular distribution of the interference effect of a stack without absorption and with absorption.

Both figures shows the effect of K-edge absorption on the transition-radiation spectrum for 65 MeV electrons. Mylar has the L and K edges at 280eV and 530eV while aluminum has the K-edge at 1.6keV. Since there is a large increase of the absorption above the edges, by choosing the material of the foil the spectrum can be narrowed due to the sudden change in x-ray absorption at the K and L photoabsorption edges in the material.

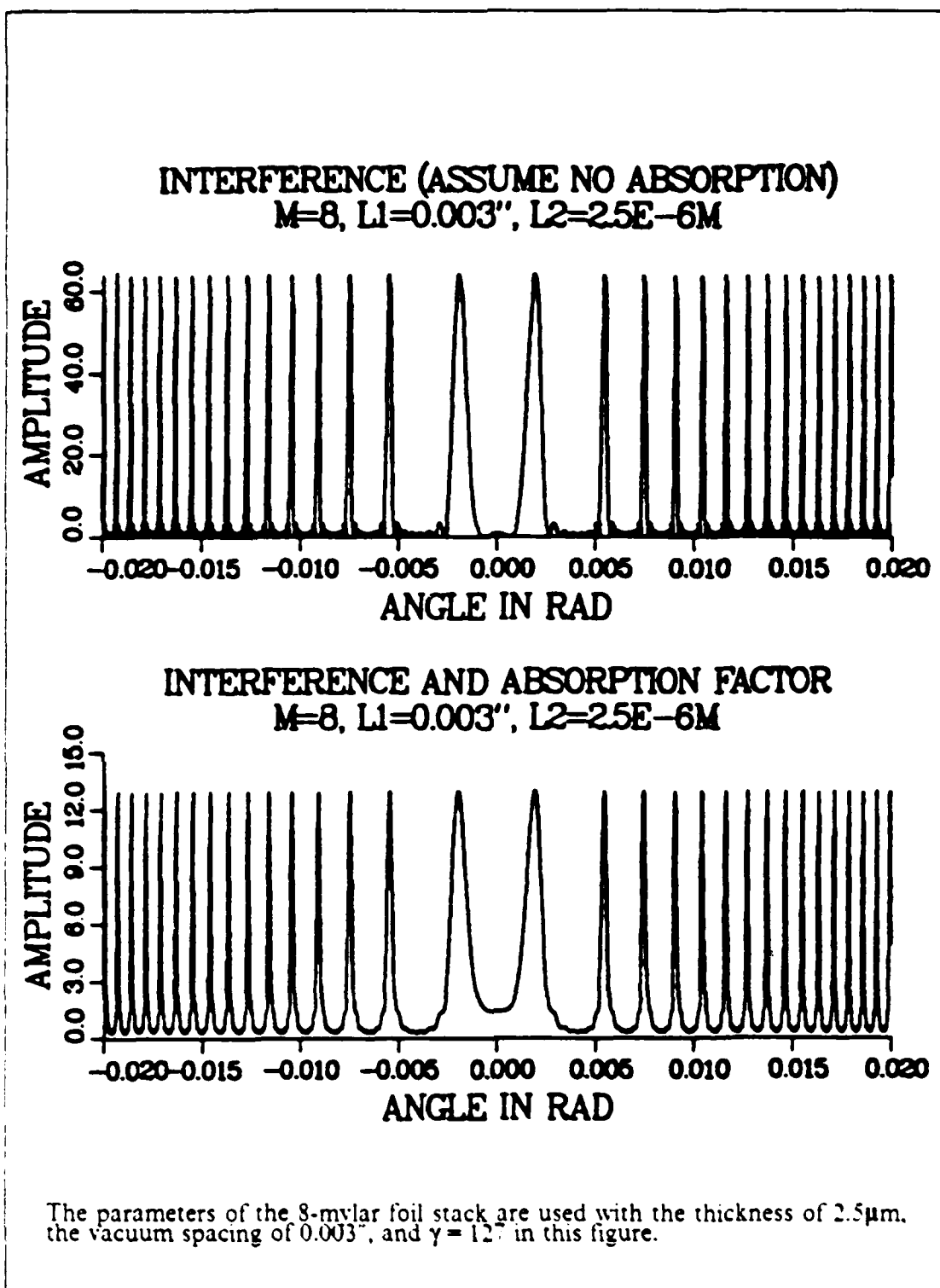## 5. Overview

The expression of the differential intensity of transition radiation is composed of three main factors as shown in Figure 2.13. As the γ varies, the radiation peak varies not only in intensity, but also in position as seen in Figure 2.8.

Figure 2.14 shows the angular distribution of the photon production by the stack of a single foil of mylar ($\omega_2 = 24.4$eV) for the various thickness, for the spacing of 0.003" and $\gamma = 127$. The spectral yield from the radiation and the peak emission angle is closely related to the thickness of the foil. The optimizing emission angle of the Figure 2.14 and 2.15 are somewhat different from the calculated value from equation 2.7 since equation 2.7 was obtained without considering the foil. In practice, to get the precise optimizing emission angle while considering the thickness of foil is very difficult. The difficulty can be overcame by the numerical methods using a computer.

Figure 2.16 shows the angular distribution of the photon production from the stacks of 4 mylar foils of the thickness of 2.5μm for $\gamma = 127$, for spacings of 0.001", 0.003" and 0.006" respectively. The intensity does not change very much depending on the spacing, but the interference pattern depends significantly on the spacing through the third term of equation 2.1 with $X = \ell_1 Z_1 + \ell_2 Z_2$. As the spacing increases, the oscillation of the radiation becomes rapid considerably and the angular width decreases.

When the absorption of the foil is negligible, the intensity of the photon production is closely proportional to the square of the number of interfaces (2M) as shown in Figure 2.17 which is plotted from the equation 2.10 for the $E = 1.2$eV. For the soft x-ray region the absorption through the medium should be considered as mentioned previously.

Figure 2.18 shows the angular distribution of the photon production through the mylar for the various number of foils, for the radiation frequency $E = 1.2$ eV, the foil thickness of 2.5 μm, the spacing 0.003" and $\gamma = 127$. The intensity of the photon production does not increase in proportion to the square of the number of interfaces,

31
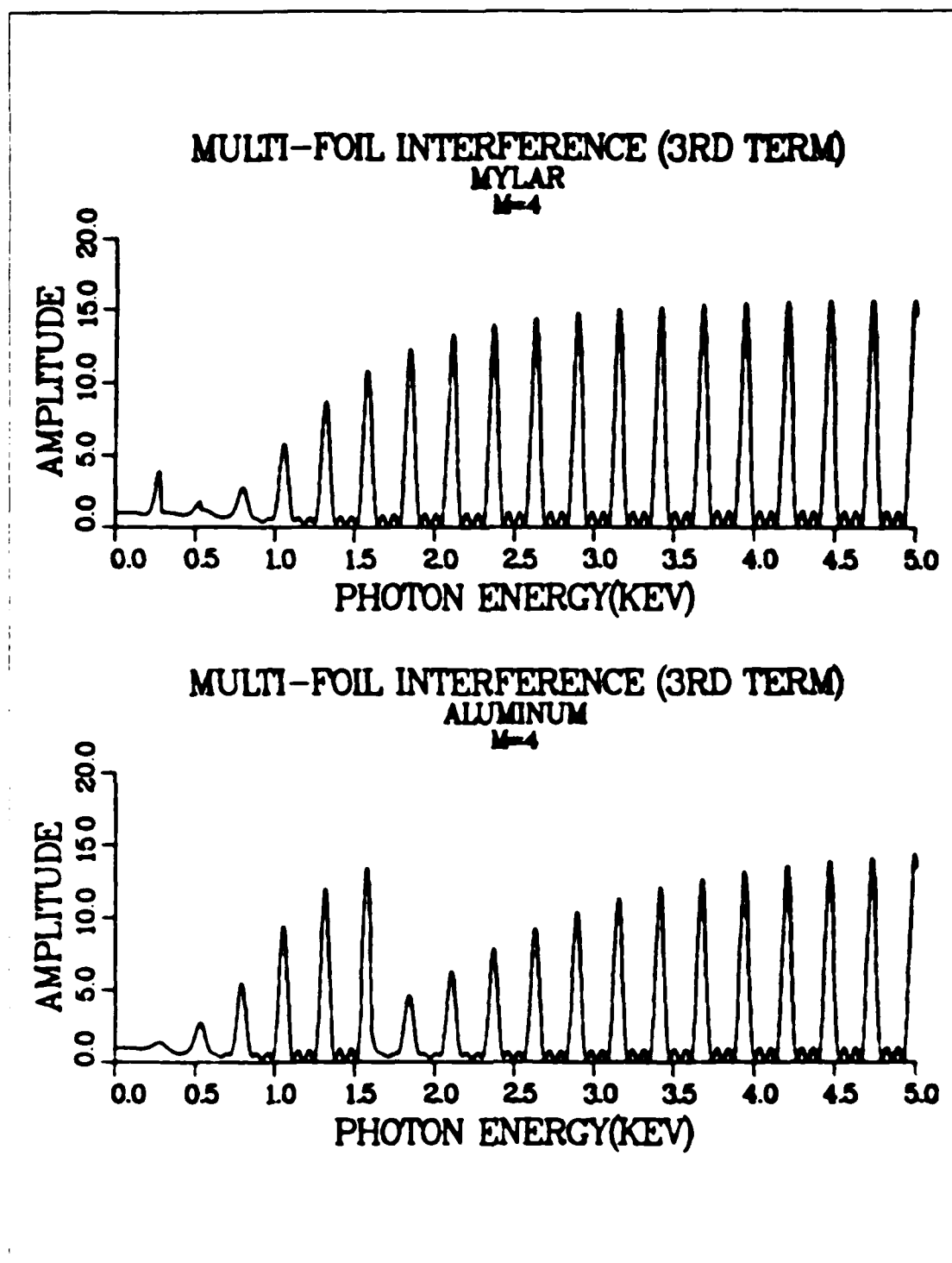
Figure 2.12   Interference and absorption with the different materials.

FIRST TERM (ANGULAR DISTRIBUTION)

2ND TERM (SINGLE FOIL INTERFERENCE)

M=8, L1=0.003", L2=2.5E-6M

The mylar foil thickness is 2.5μm, the vacuum spacing is 0.003", and $\gamma = 127$ for this graph.
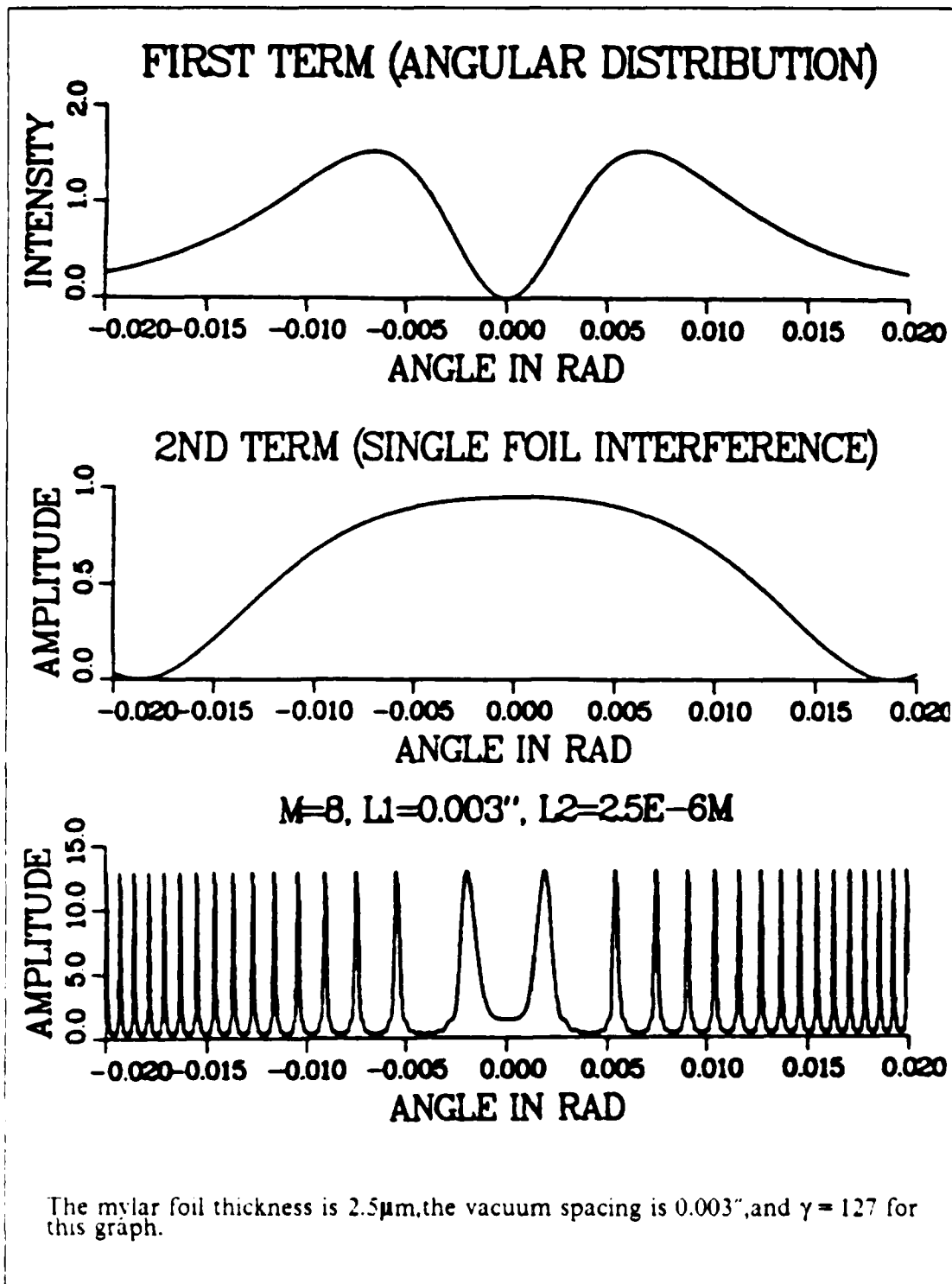
Figure 2.13   Comparison of contribution factor to the angular distribution of the photon production.

since as the number of foils increases, the loss due to x-ray absorption also increases, but the increase will stop at a certain number of foils because of the equation 2.26. The angular structure becomes progressively narrower as the number of foils increases, but there is no significant shift of the angular position of the each structure.
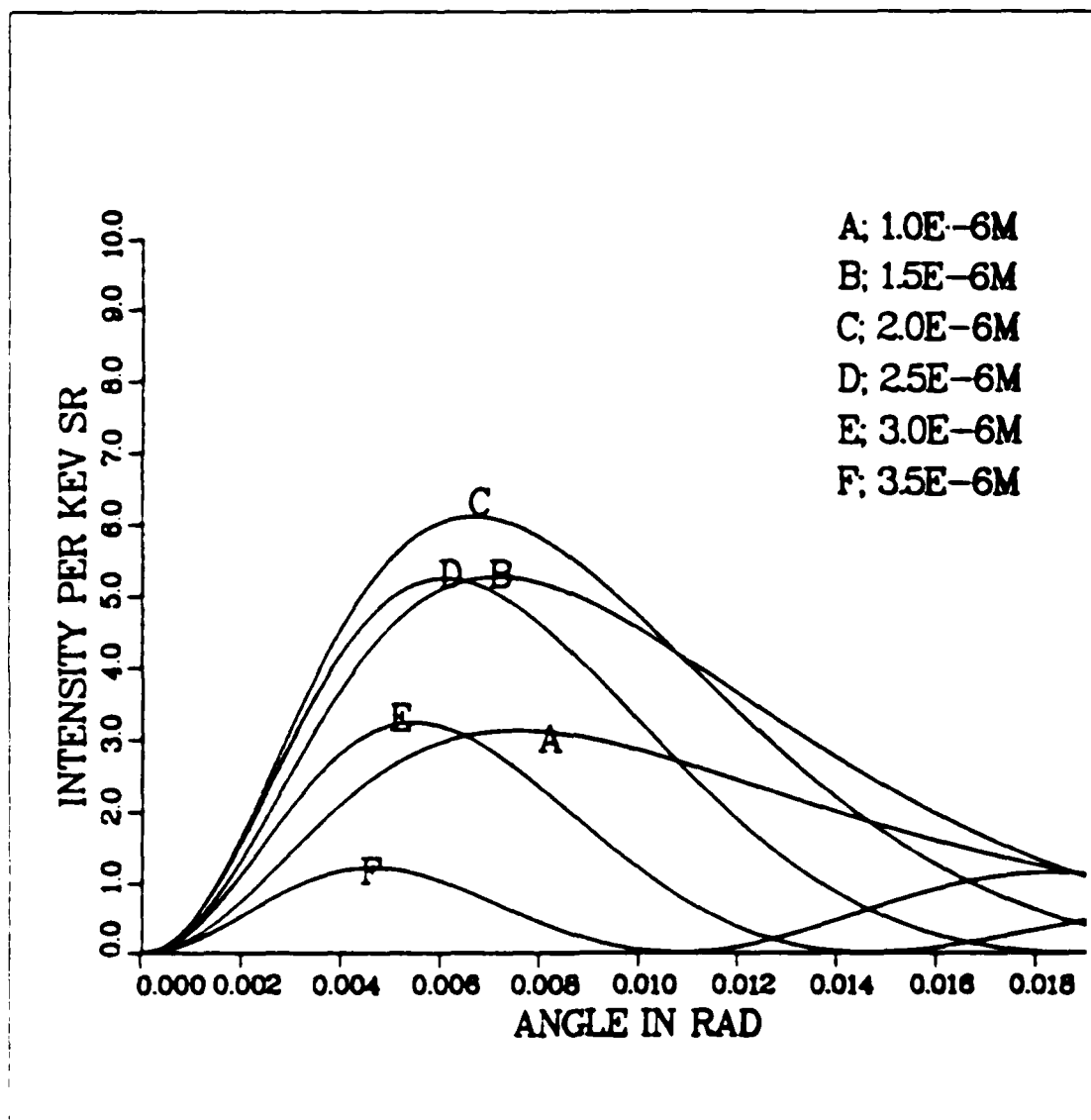
Figure 2.14   Comparison of the angular distribution of the photon production produced by the various thickness of a single foil.
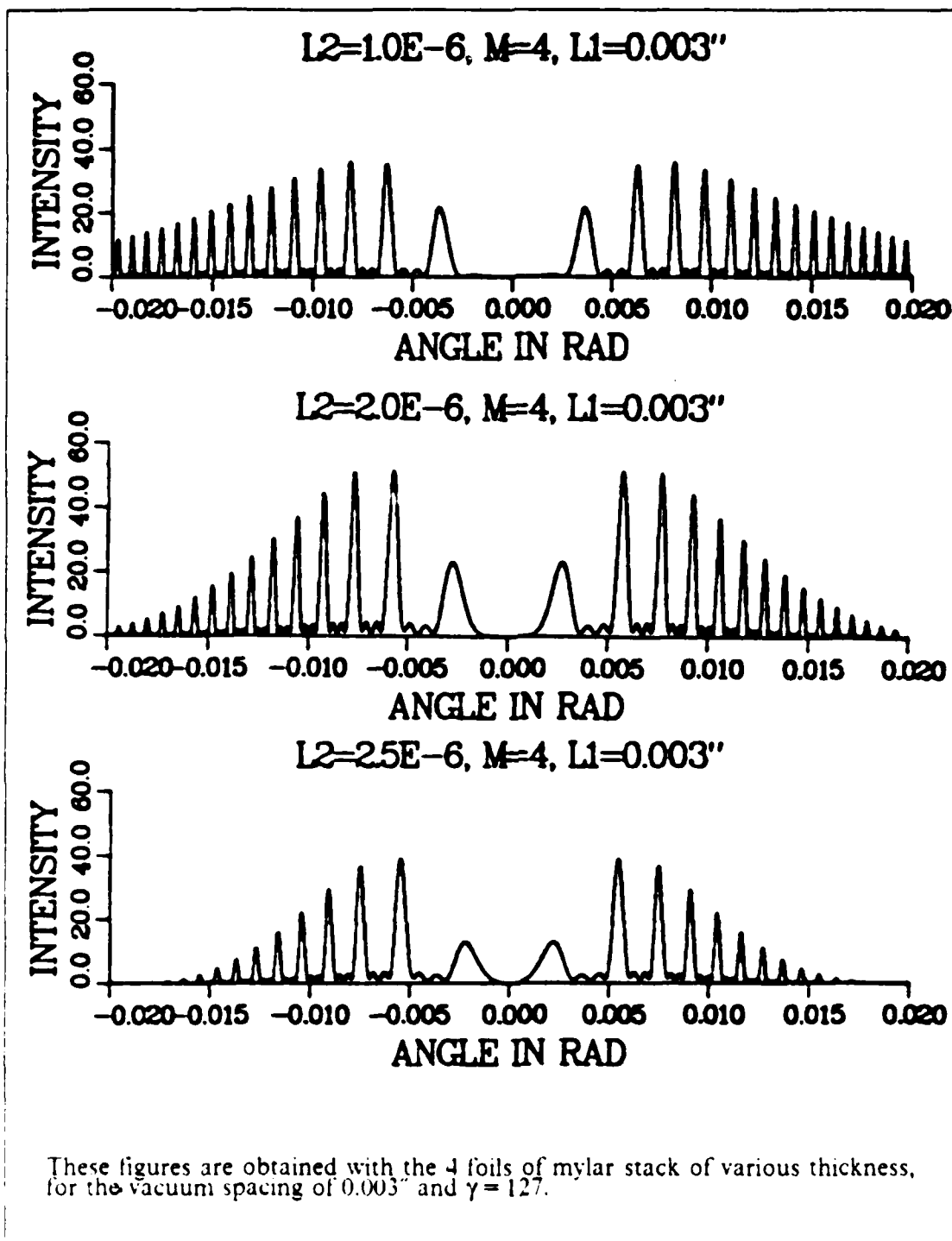
Figure 2.15 Angular distribution of the photon production produced by the stack of various thickness of foils.
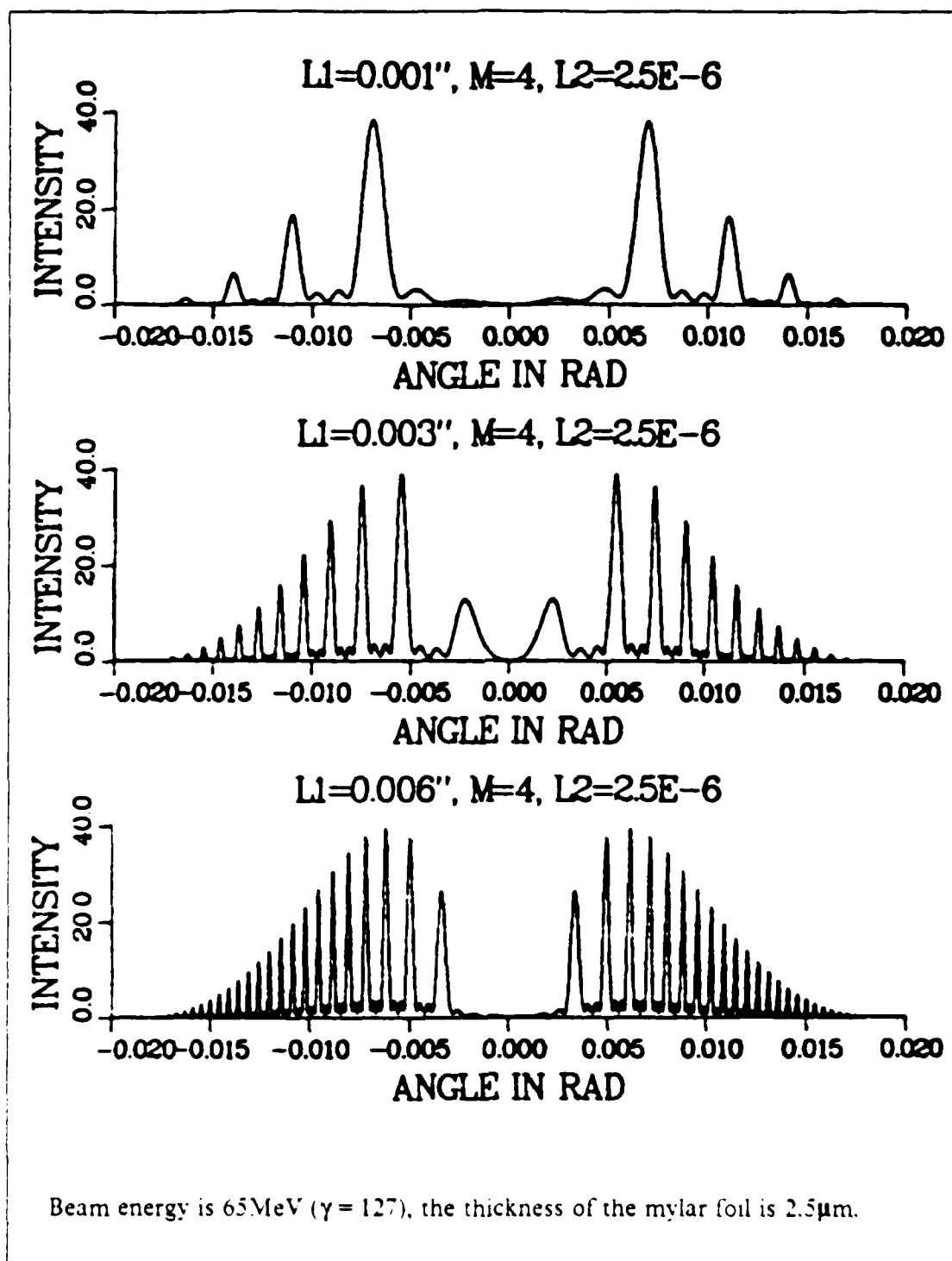
Figure 2.16 Angular distribution of the photon production produced by the stack of various spacing.
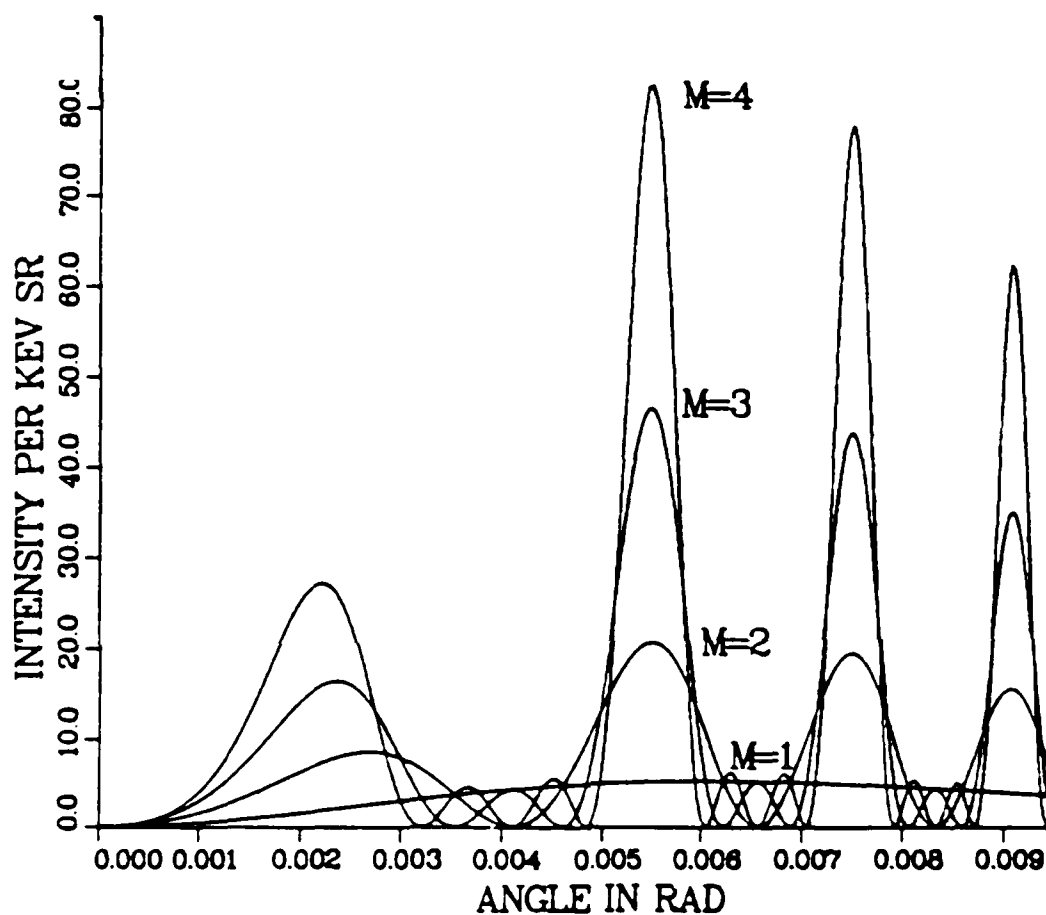
These curves show the change of the theoretical x-ray production from the stacks of various number of mylar foils for the thickness of $2.5\mu m$, the vacuum spacing of $0.003''$, and the beam energy is 65MeV. The absorption of the mylar foil and vacuum spacing are assumed to be negligible so that the peak of the radiation increases as the square of the number of foils.

Figure 2.17   Comparison of the angular distribution of the photon production produced by the stack of various number of foils.

Mylar stacks with $\ell_2 = 2.5\mu m$ and $\ell_1 = 0.003"$ are used. $\gamma = 127$, $\sigma \neq 0$.
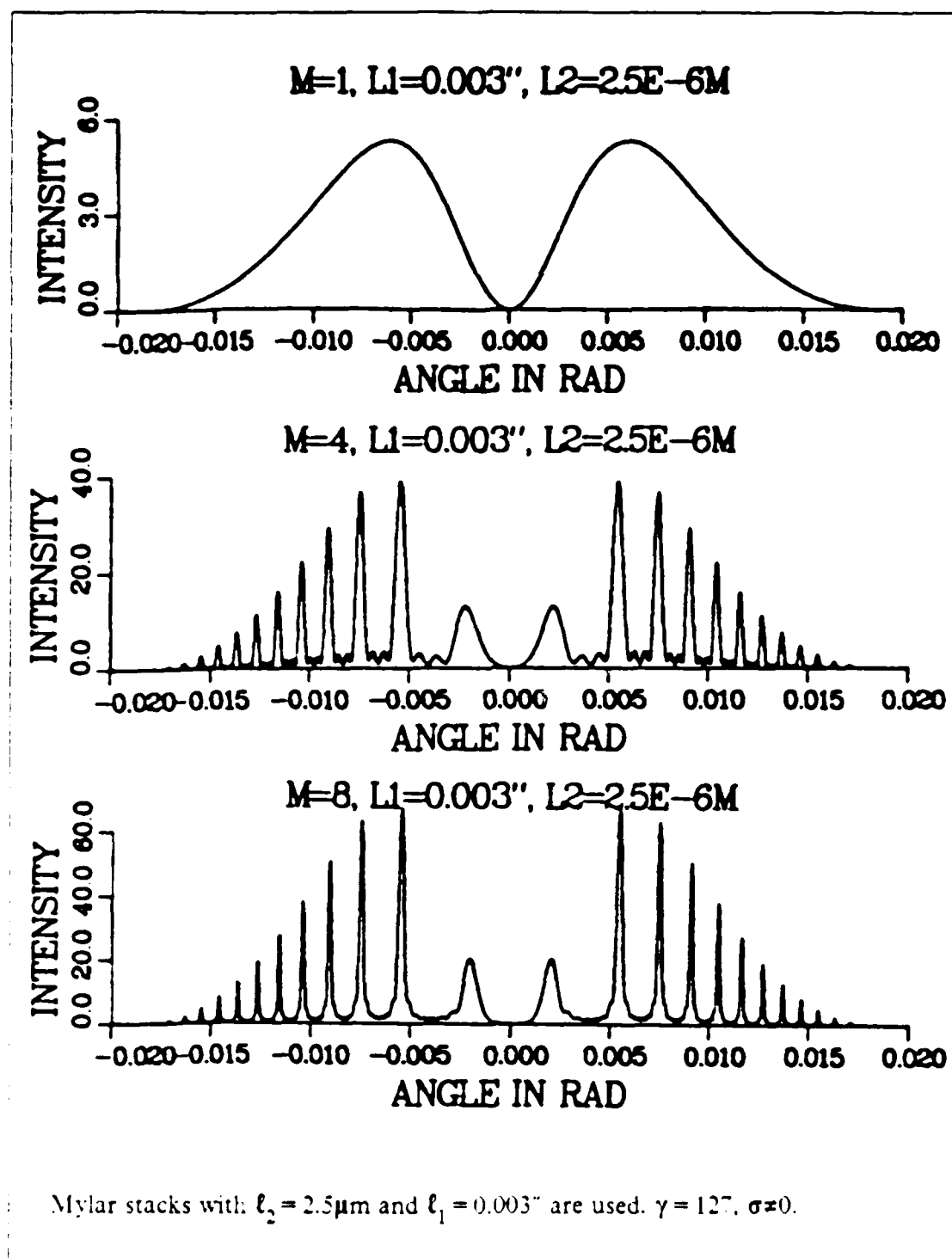
Figure 2.18   Angular distribution of the photon production produced by the stack of various number of foils.

III. THE EXPERIMENT

A. EXPERIMENTAL SETUP

This experiment was performed using medium energy charged particles produced by the electron linear accelerator (LINAC) at the Naval Postgraduate School (see Appendix B for detailed information). Figure 3.1 shows a schematic diagram of the experimental apparatus. The electrons emerge from the LINAC into the experimental chamber which contains the foil stack and the x-ray detector. After exiting the experimental chamber the electrons strike the scintillation detector connected to the integrator before entering the beam dump.
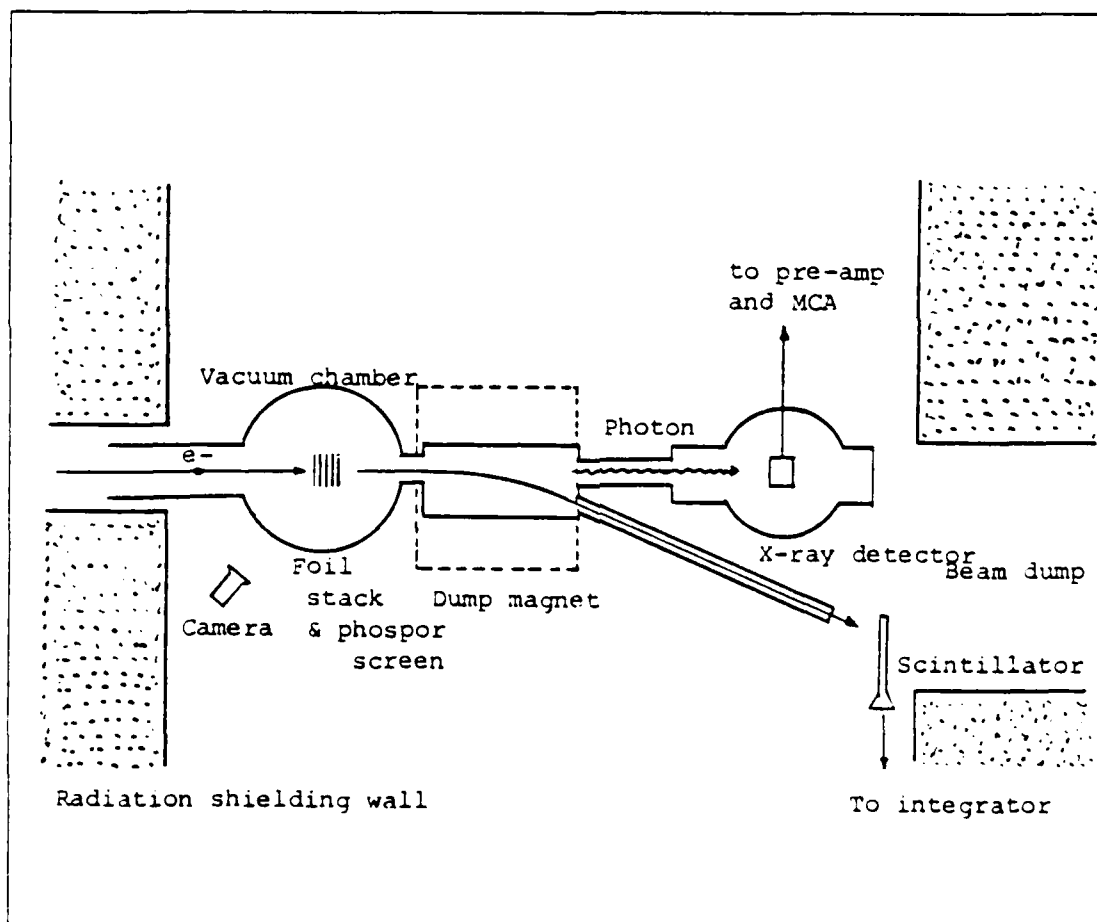
Figure 3.1   Diagram of the experimental apparatus.

Figure 3.2   Dump magnets.

A permanent magnet and an electro-magnet were used to bend the electron beam after passing through the stack for the first time. It is necessary to bend the charged particle beam out of the forward cone of the transition radiation with a strong magnetic field when using an x-ray detector, since both particle and the transition x-rays traverse the detector window simultaneously, unless the particle is deflected after passing through the stack. The red colored strong permanent magnet was set to bend the electron beam out 20°. Phosphor screens were set inside the chamber and in the front of the dump hole in order to trace and align the electron beam. Figure 3.2 shows the dump magnets, which is the red colored strong permanent magnet used in the experiment.

A flowing gas x-ray detector manufactured by the Manson company was used to detect the photons produced as transition radiation. A photograph of the detector is

shown in Figure 3.3. The electrons which are separated from the gas molecules by the absorption of a photon gain energy from the collision and the electric field as shown in Figure C.1. The detector is comprised of a central anode wire surrounded by a cylindrical cathode which is grounded. Since the field near the anode varies inversely as the radial coordinate of the electron, the energy gained between collisions from the field rapidly increases as the electron approaches the anode.

The performance characteristics of the detector depend on the gas pressure, therefore constant gas pressure is important during a set of experiments. More detailed information about the Manson gas flow x-ray detector is given in Appendix C.

In order to monitor and assure the constant total charge for each measurement, the scintillator seen in Figure 3.4 was mounted behind the proportional counter and an integrator was used as shown in Figure 3.5. The integrator accepts either pulsed or continuous currents as an input and produces a series of digital output pulses whose number is linearly proportional to the accumulated charge. These output pulses are connected to the multichannel analyzer to control it externally by the dwell time during scanning.

The multichannel analyzer used in this experiment has data processing capabilities. It performs in two analysis modes:

(1)   Pulse Height Analysis (PHA) mode gives the frequency distribution of spectrum.

(2)   Multichannel scaling (MCA) mode gives the angular or spatial distribution.

A block diagram of the electronics apparatus is shown in Figure 3.6.

For this experiment, mylar stacks with thickness of 2.5μm were designed and constructed as shown in Figure 3.7 and in Appendix D. These 2.5μm mylars were separated by 0.003" shim steels and 0.001" shim steels. The assembly itself is relatively easy. All the difficulties were caused by the very thin spacer and mylars, but ventilating holes in the steel shims were not necessary. The mounted stacks for this experiment are all shown in Figure 3.8.

B.   PROCEDURE

The first step of this experiment was done to investigate the frequency distribution of transition radiation, and the second step of the experiment was to study the angular distribution of the transition radiation and coherent addition effect. The experimental arrangement is similar to that used in [Ref. 7: p.1775].
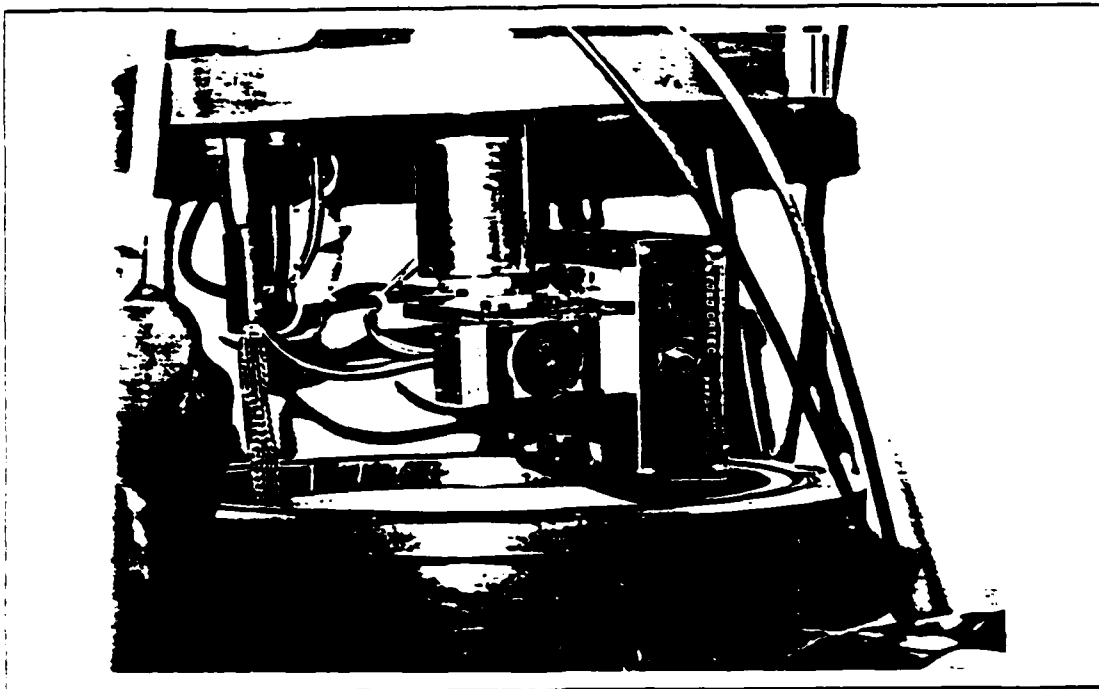
Figure 3.3   Manson gas flow x-ray detector.
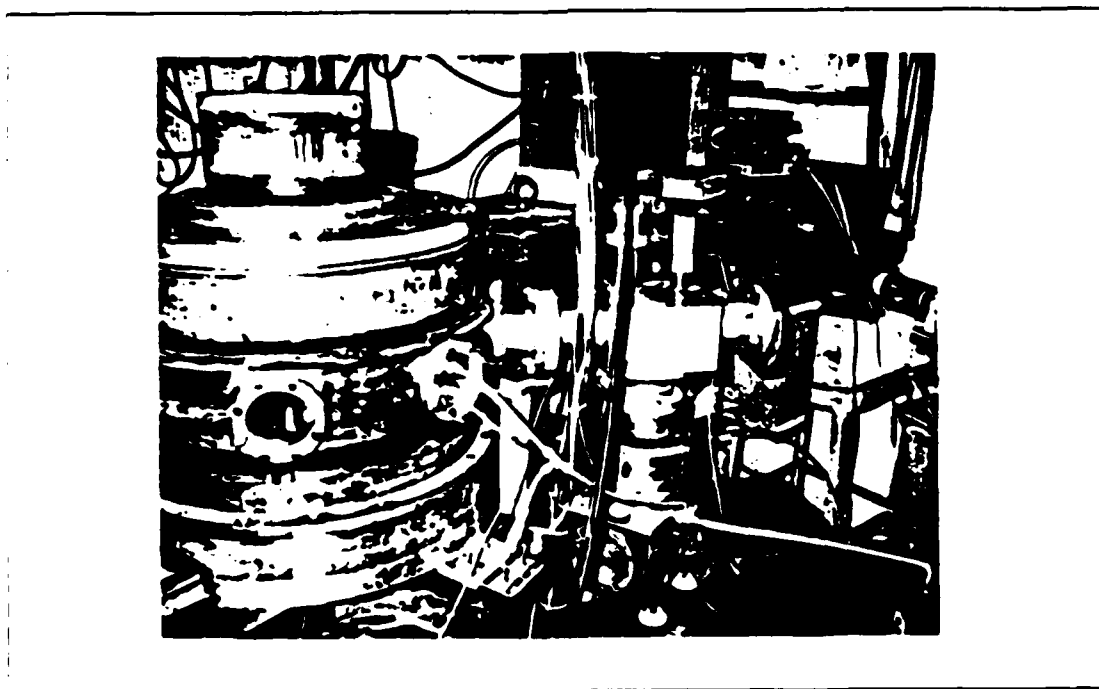
Figure 3.4   Target chamber and scintillator.
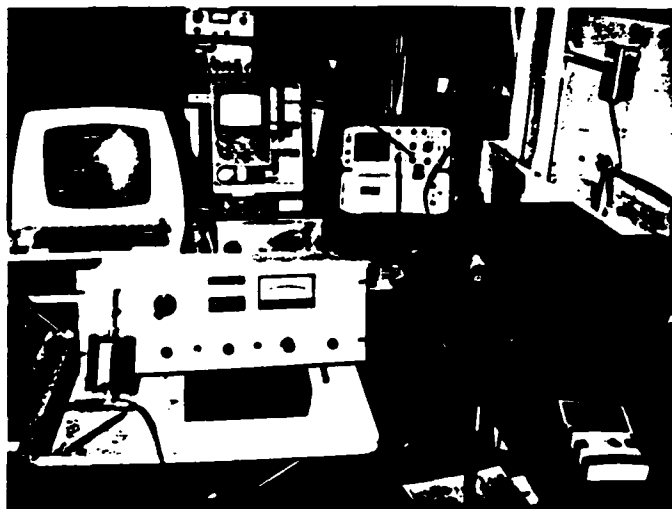
This Figure shows MCA, high voltage supply, oscilloscope, integrator, and a computer terminal to control the speed of motor driving.

Figure 3.5 Control room arrangement.

As shown in Figure 3.1, accelerated electrons enter from the left-hand side of Figure 3.1 to a target chamber, where they pass through the foil stack and a permanent magnet. the electron beam is deflected by a dump magnet out of the forward cone of transition radiation and away from the proportional counter, and then the beam goes through the scintillator and is absorbed into the beam dumping earth.

First of all. calibration of the detector position was required in order to determine the relation between the digital counts of the motor driver and the actual position or angle of the detector window. The calibration of the detector position was 80 turns per inch movement.

An Fe^{55} radioactive source, which radiates 6keV x-rays and has a 3keV escape peak (as will be seen in the next chapter) was used to calibrate the peak of the x-ray spectrum. These two peaks give the calibration of the multichannel analyzer, actually of the pulse height analyzer (PHA) in this case. Using this calibration, the energy level of each spectrum peak from different kind of stacks could be easily calculated.

43
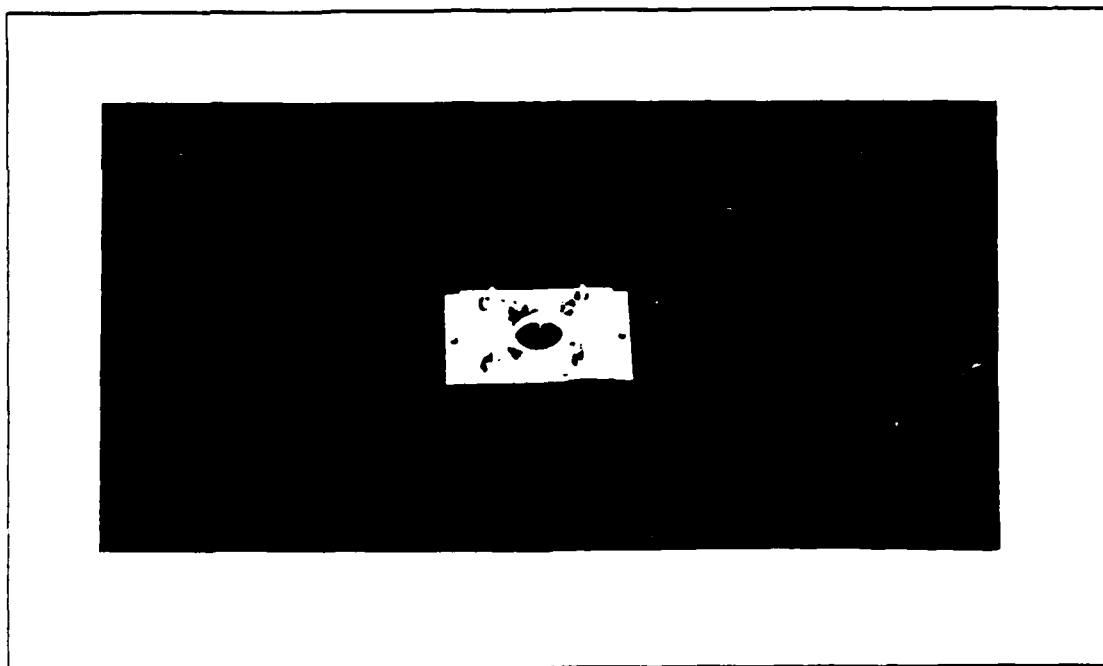
Figure 3.7   Mylar stack constructed.
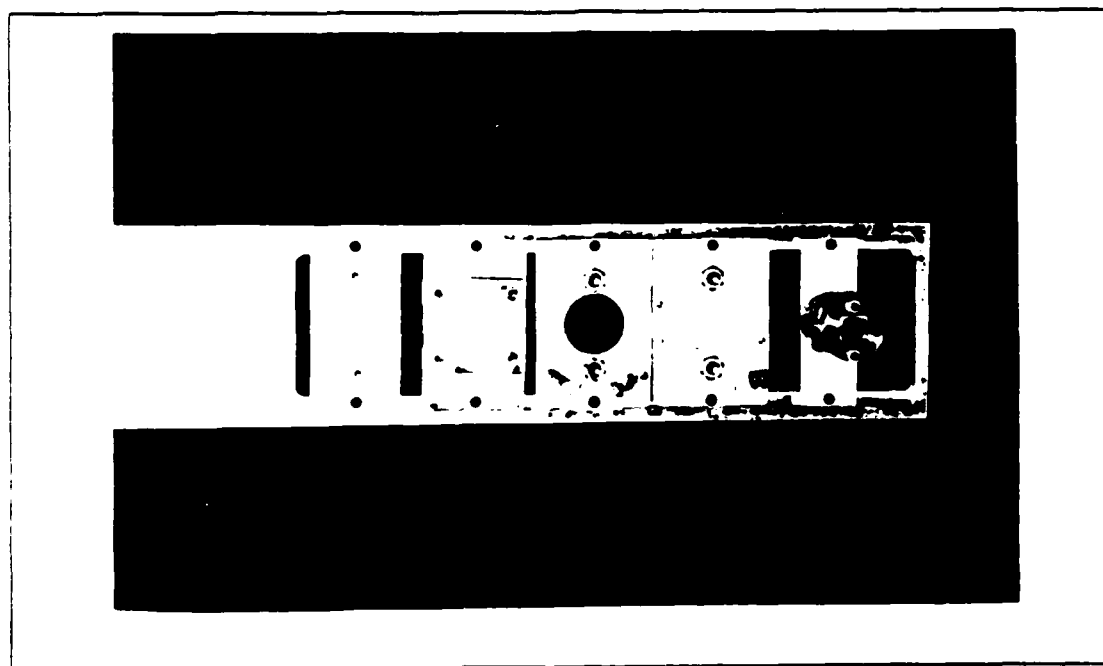
Figure 3.8   Mount of stacks.
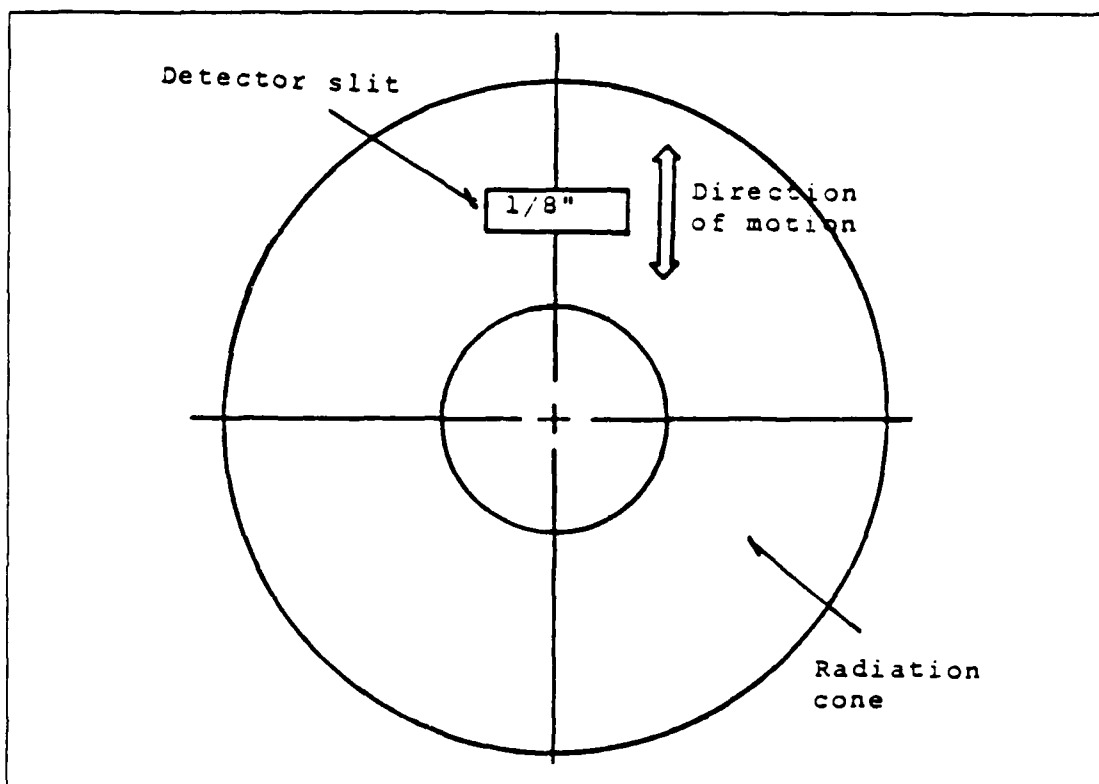
Figure 3.9   Schematic diagram of scanning.

Before scanning, the MCA was set in the mode of multichannel scaling (MCA) to obtain the curve representing frequency of occurance vs. elapsed time. This MCS analysis is very well programmed to study this particular distribution of events vs. time, here the time means the dwell time which is governed by the integrator. Then the detector was moved up and down between the calculated edges of the radiation cone passing through the center, allowing the transition radiation cones to be scanned as shown in Figure 3.9. For the detector to resolve the cone of radiation, the dimension of the detector slit should be small relatively to the dimension of the cone radius. Since it was relatively large with a width of 1 8", a collimator with a hole of 3 32" was designed and tested. At first, Al was used as a material for the collimator, but x-ray fluorescence gave another problem. This will be discussed in the next chapter. Therefore to stop the x-ray fluorescence the collimator was made of lead.

IV. RESULTS AND CONCLUSIONS

A. RESULTS

The spectrum from the Fe^{55}, which has 3keV and 6keV peaks, is shown in Figure 4.1. Figure 4.2 shows the measured spectrum from a stack of 8 mylar foils, each with a thickness of 2.5μm. The peak of the spectrum shown in Figure 4.2 is 1.8keV.

Figure 4.3 shows the measured angular distribution with the stack of 8 mylar foils which has a spacing of 0.003" and thickness of 2.5 μm, for the beam energy of 65MeV.
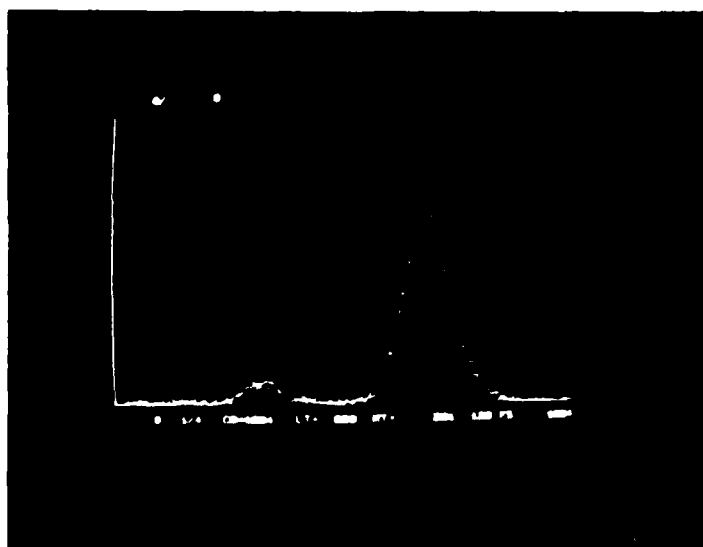
The absolute number of photons are not represented in this figure. Gas pressure is 328 Torr.

Figure 4.1 Spectrum obtained from Fe^{55}.

47
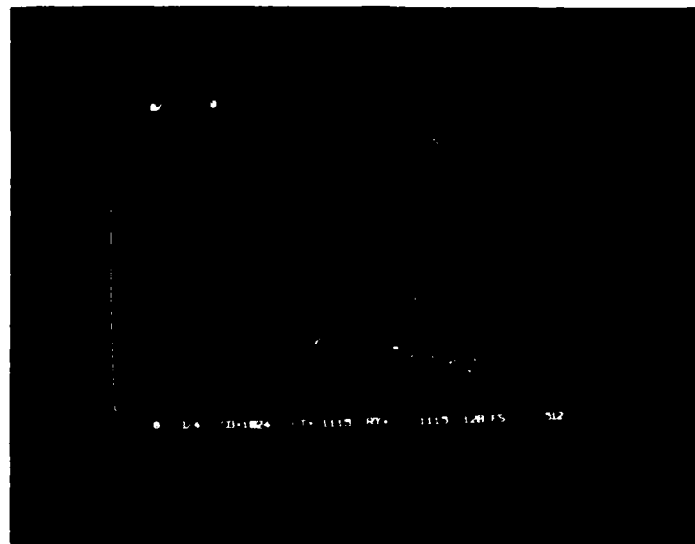
The thickness of the foil is 2.5μm and the beam energy is 65MeV. The spectrum will be discriminated against for energies less than 0.5keV and larger than 3.5keV, since those portions are composed of large amounts of background noise. Only the energy range between 0.5keV and 3.5keV will be used for scanning.

Figure 4.2   Spectrum obtained from the stack of 8 mylar foils.

The center of the cone was not seen in this case. The possible reasons for that are:

(1)   The size of the detector window as seen in Figure C.2 was not small enough to resolve the valley at the center. It was 2.3 mrad x 7.5mrad.

(2)   The detector might be shaded by the edge of the narrow (1.25" diameter) pipe as seen in Figure 3.1.

In order to avoid these problems, a 3/32" diameter iris was installed on the proportional counter, and the beam energy was increased from 65MeV to 98MeV. The latter reduced the size of the transition radiation cone allowing the cone to pass unobstructed through the narrow pipe. Thus the transition radiation cone was observed as seen in Figure 4.4. This is the second observation of the cone of transition radiation [Ref. 10].
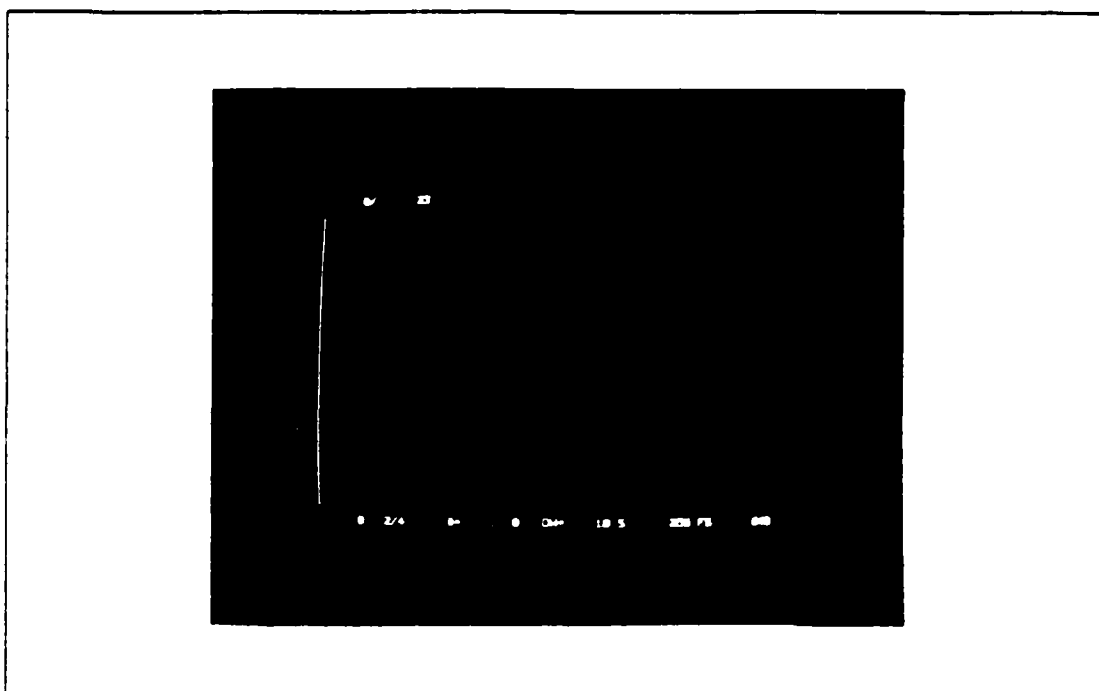
Figure 4.3   Measured angular distribution with $\gamma = 127$.
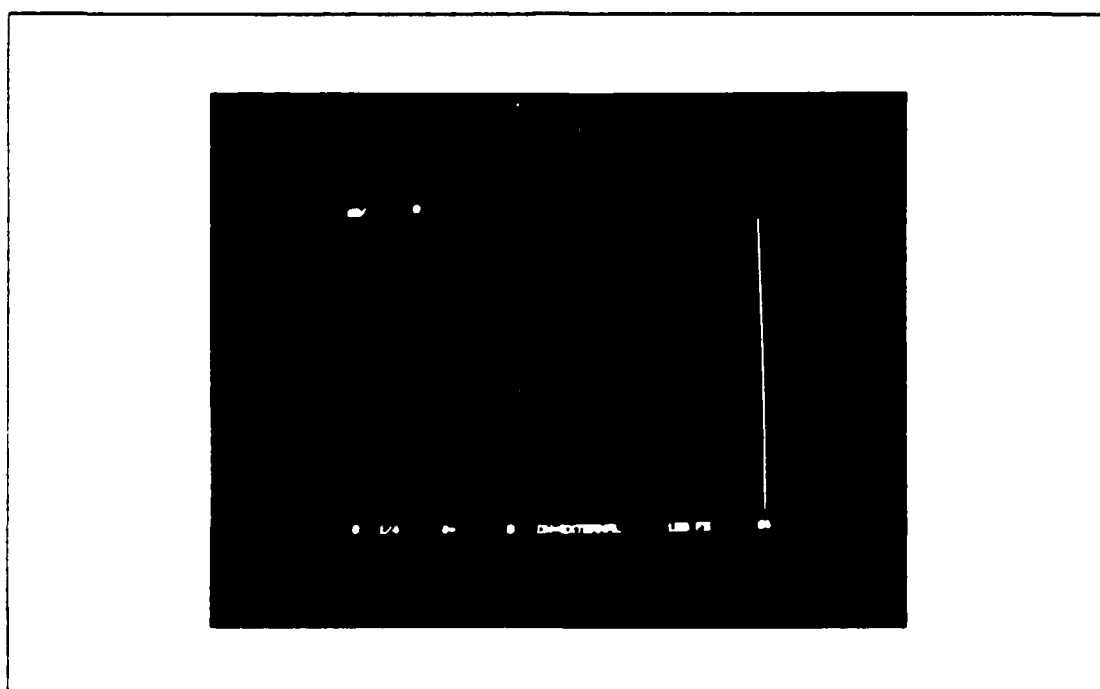
Figure 4.4   Measured angular distribution with $\gamma = 191$.

49

TABLE 2
COMPARISON OF THE ANGLES OF THE CONE

M	γ	peak photon enenergy	calculated peak angle	measured peak angle
8	127	1.38keV	6.4mrad	5.8mrad
8	191	1.80keV	4.4mrad	4.7mrad

Table 2 lists the peak angles with respect to the electron beam axis, which are measured from Figures 4.3 and 4.4, and compares them with the values calculated from equation 2.6. The measured peak values match the calculated values within 10 % error.

The measured curves for the periodic stacks shown in Figures 4.3 and 4.4 do not show the coherence effect predicted in the Chapter II with possibly two exceptions. Several peaks were observed, as shown in Figure 4.4. However, these were not reproducible. Possible reasons for not seeing the resonance effect more clearly are listed in the next section.

The predicted angular distribution curves should not necessarily fit the measured curve in the experiment, since in the experiment the photon energy was integrated from 500eV up to 3500eV while in the prediction a photon energy near the peak of the spectral distribution was selected. The computer program should expand to include this integration.

B. CONCLUSIONS

The transition radiation cone as measured in these experiments confirms the theoretical predictions quite well even though there is the possibility of the detector not passing through the central axis of the cone.

At the lower electron beam energies the cone was not seen. This further indicates that elastic scattering affected the resonance effect since the scattering is greater at lower electron energies.

The fine structure of the angular distribution of the radiation could not be resolved. Possible reasons for not seeing the coherence effect are:

(1)   The electrons are being elastically scattered by the foils causing the photons to go off in the different directions, thus there is no phase addition.

(2)   Inaccuracy of the foil thickness and nonuniformity of the steel spacing caused by the wrinkles in the foils prevent the phase addition between foils.

(3)   Angular resolution of the detector may have been larger than the angular width of the spikes.

This work may have several possible applications to particle beam diagnostics. For example:

(1)   The peak to valley ratio of the resonance cone of the transition radiation can be used to monitor the electron beam emittance, since the ratio approaches unity when the divergence of the beam increases [Refs. 1,6].

(2)   The apex angle, which has a strong dependence of the beam energy, can be used to measure the absolute beam energy by using equation 2.7, $\theta_{opt} \sim 1/\gamma$.

For further work on this topic, suggestions for improving the experiment are:

(1)   The separation between the foils of the stack and the dimension of the detector window should be small enough to be able to resolve the fine structure from the interference phenomena.

(2)   In order to obtain the proper number of points for the angular distribution curve, very slow movement of the position of the detector is required.

(3)   The operating condition of the accelerator should be stable. For example: the ratio of the electrons to machine pulse and the pressure of the gas in the Manson gas flow detector chamber.

(4)   To get a usable radiation cone, the detector should pass the center of the radiation cone.

(5)   The beam should be traced and well collimated. Also the diameter of the pipe where the produced photons pass through to the x-ray detector should be large enough not to make any shadow into the cone of x-ray production.

APPENDIX A

EXAMPLE PROGRAM FOR GRAPHIC ANALYSIS

```fortran
C
C
C        ****************************************************
C        *****   This fortran program is to analyze      *****
C        *****   the angular distribution of the x-ray   *****
C        *****   transition radiation by the graphical   *****
C        *****   method with the tektronix 618           *****
C        ****************************************************
C
C
C        *****          HERE MAIN PROGRAM BEGINS         *****
C
         DIMENSION Z1(4001),Z2(4001),A1(4001),TH(4002),F1(4001)
         DIMENSION F2(4001),F3(4001),X(4001)
         REAL XM,XL1,XL2,E,XMU,SIG,EP,GA
C
C        *****      THE PARAMETER BELOW CAN BE CHANGED    *****
C
         XM=4.
C        XL1=2.54E-5
         XL1=7.62E-5
C        XL1=15.24E-5
         XL2=2.5E-6
C        EP=15.8E-3
         EP=24.4E-3
         GA=127.0
         E=1.2
         th(1)=-0.02
C
         DO 10 I=1,4001
C        ***** formation lengths of spacing and foil *****
            Z1(I)=6.586E-10/(1.0/GA**2+TH(I)**2)
            Z2(I)=6.586E-10/(1.0/GA**2+(EP/1.2)**2+TH(I)**2)
C        ***** single interface intensity *****
            F1(I)=1.421E15*(Z1(I)-Z2(I))**2*(SIN(TH(I)))**2
C        ***** single foil interference *****
            F2(I)=(SIN(2.5E-6/Z2(I)))**2
            X(I)=7.62E-5/Z1(I)+2.5E-6/Z2(I)
C
C        ***** pure interference term for NEGLIGIBLE ABSORPTION *****
C
            F3(I)=(SIN(XM*X(I))/SIN(X(I)))**2
C
C        ***** CONSIDERING THE ABSORPTION COEFFICIENT OF MYLAR *****
C
            IF (E.LE. 0.28) THEN
                XMU=6.975E6*(E/0.1)**(-2.67)
            ELSEIF (E.GT. 0.28 .AND. E.LE.0.53 ) THEN
                XMU=4.6E6*(E/0.28)**(-2.28)
            ELSEIF (E.GT. 0.53.AND. E.LE.3.4) THEN
                XMU=2.09E6*(E/0.53)**(-2.70)
            ELSEIF (E.GT.3.4 .AND. E.LE.10.0) THEN
                XMU=1.395E4*(E/3.4)**(-3.13)
            ENDIF
C
C        ***** CONSIDERING THE ABSORPTION COEFFICIENT OF ALUMINUM *****
C
            IF (E(I).LE. 0.5) THEN
                XMU=7.020E6*(E(I)/0.1)**(-1.05)
            ELSEIF (E(I).GT. 0.50 .AND. E(I).LE.0.80 ) THEN
                XMU=1.296E6*(E(I)/0.50)**(-1.76)
            ELSEIF (E(I).GT. 0.80.AND. E(I).LE.1.6) THEN
```

```fortran
            XMU=0.567E6*(E(I)/0.80)**(-2.91)
         ELSEIF (E(I).GT.1.6 .AND. E(I).LE.10.0) THEN
            XMU=1.026E6*(E(I)/1.6)**(-2.72)
         ENDIF
C
C        ***** calculation of interference and absorption term *****
C
         SIG=XL2*XMU
         F3(I)=(1.+EXP(-XM*SIG)-2.*EXP(-XM*SIG/2.)*COS(2.*XM*X(I)))
     +   /(1.+EXP(-SIG)-2.*EXP(-SIG/2.)*COS(2.*X(I)))
C        ***** average absorption term *****
C        F3(I)=(1-EXP(-XM*SIG))/SIG
C        ***** differential intensity  *****
         A1(I)=4.000*F1(I)*F2(I)*F3(I)
C        ***** high resolvable increment of angle in radian *****
         TH(I+1)=TH(I)+1.0/100000.0
10       CONTINUE
C
C
C
C        *************** GRAPH BEGINS HERE ******************
C
         CALL TEK618
C
C        *** AREA DEFINITION ***
C
         CALL PAGE(15.,11.)
         CALL NOBRDR
C
         CALL AREA2D(8.5,2.)
C        CALL FRAME
C        cALL THKFRM(.006)
C
C        *** LETTERING ***
C
         CALL COMPLX
C
         CALL MX1ALF('STANDARD','#')
         CALL MX2ALF('L/CSTD','/')
         CALL MX3ALF('ITALIC','%')
C
         CALL HEIGHT(0.25)
C
         CALL HEADIN('ANGULAR DISTRIBUTION$',100,1.5,2)
         CALL HEADIN('M=25, L1=0.003",  L2=2.5E-6M$',100,1.0,1)
         CALL XNAME('ANGLE IN RADS',100)
         CALL YNAME('INTENSITY$',100)
C
C        *** GRID DEFINITION ***
           CALL GRAF(-0.02,0.005,0.02,0,40.,80.)
C m=25 CALL GRAF(-0.02,0.005,0.02,0,2.5E3,5.0E3)
C
C        CALL DOT
C        CALL GRID(1,1)
C        CALL RESET('DOT')
C
C        ***     CURVE DRAWING     ***
C
         CALL CURVE(TH,A1,801,0)
C
C        *** END PLOTTING ***
C
C
         CALL DONEPL
C
         STOP
         END
```

APPENDIX B
LINEAR ACCELERATOR IN THE NPS

The electron linear accelerator is used for the study of nuclear structure, radiation damage and coherent radiation. This facility is operated for the medium energy range from 15 MeV up to 100 MeV. Figure B.1 shows the linear accelerator experimental station, and the characteristics of the LINAC is shown in Table 3.
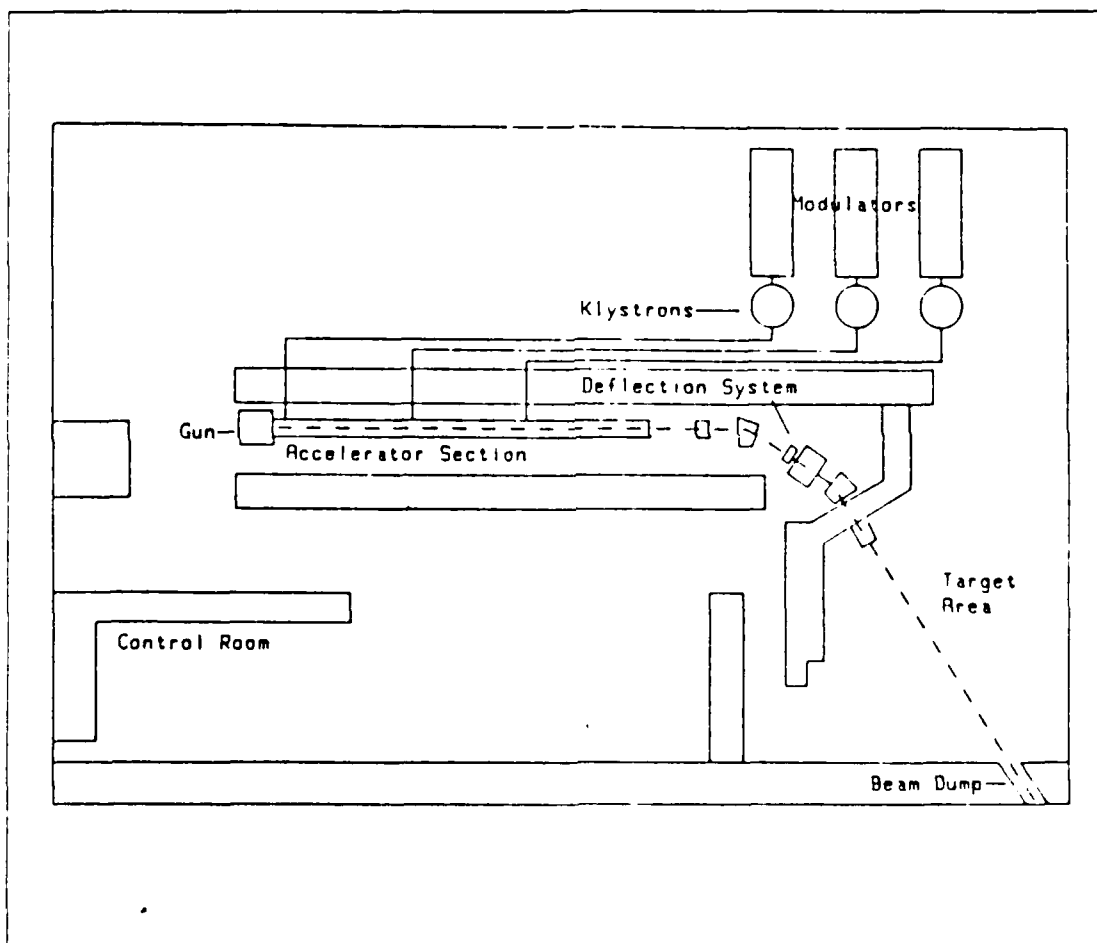
Figure B.1 NPS 100MeV linear accelerator experimental station.

TABLE 3
LINAC SPECIFICATIONS

Maximum beam energy	120	MeV
Average electron current	0.3	μA
Pulse duration	1.5	μs
Pulse frequency	60	Hz
Klystron peak power	21	MW
Klystron frequency	2.856	GHz
Total length of accelerator	30	ft
Number of klystron	3	

APPENDIX C

MANSON GAS FLOW X-RAY DETECTOR

The selected data to be helpful to study this experiment are shown in the following figures for reference from Manson's letters or instructions of the machine.

An anode wire which is located along the cylindrical proportional counter axis has a positive high voltage and the cathode, inside wall of cylinder is grounded. The electric field near the anode is very large in order to accelerate the separation of electron from the ion.
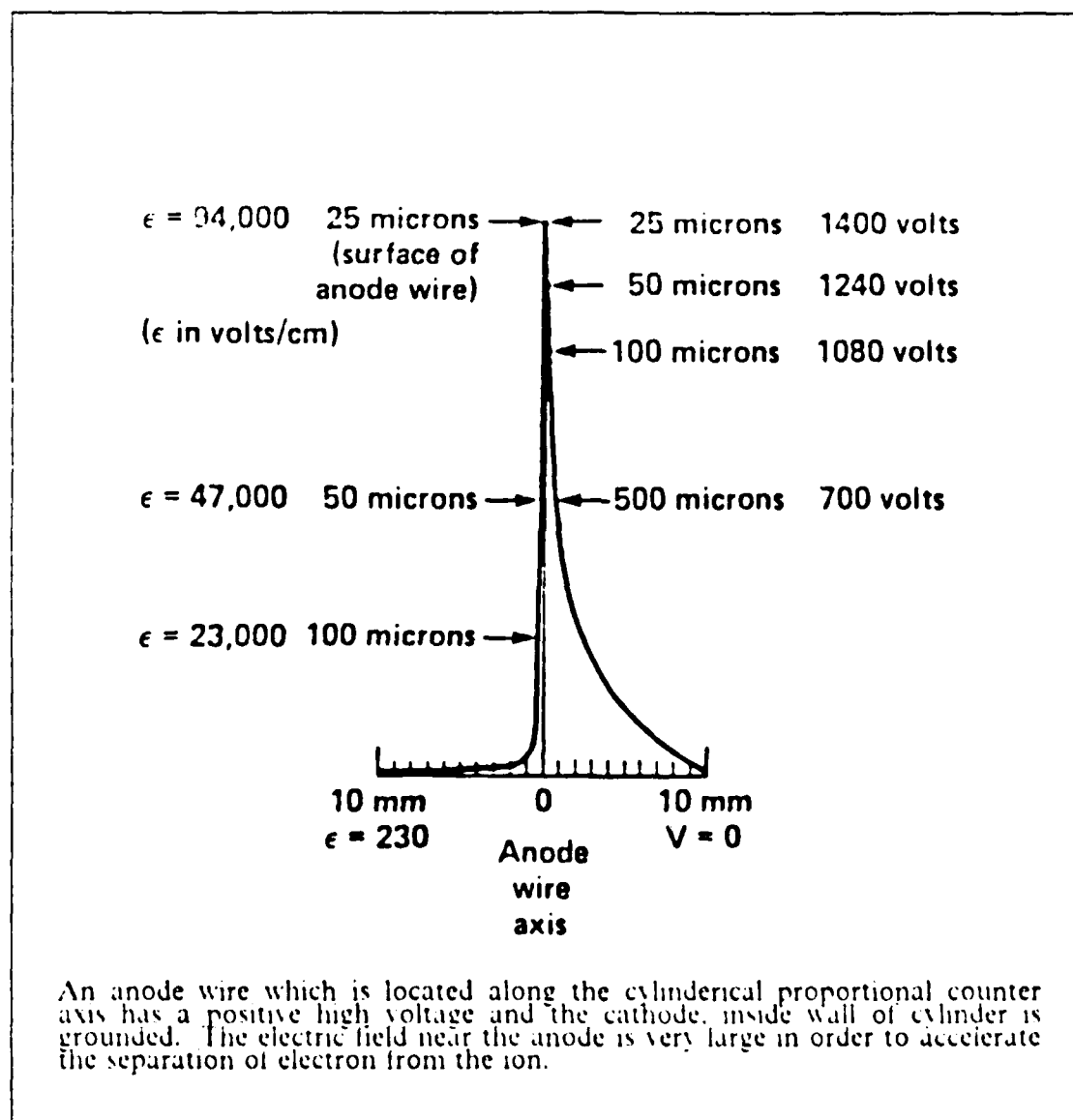
Figure C.1   Electric field strength inside the detector.
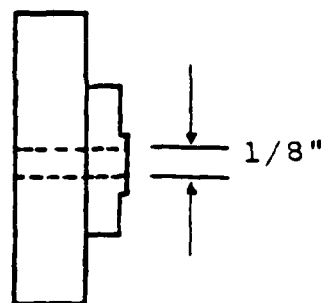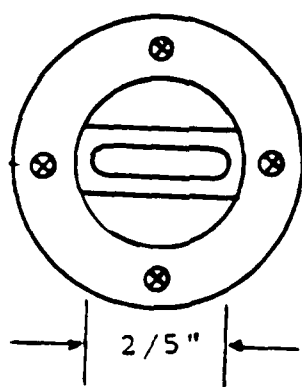
The size of the window slit is 1 8" x 2 5" which supports an operating differential pressure of 400Torr. with 800Torr maximum. Internal pressure must exceed the pressure outside of the window. The very small dimension slit is required in order to obtain high spatial resolution.

Figure C.2 Detector window.

APPENDIX D
DESIGN OF STACK

After the parameters (i.e. the foil number, the foil thickness, and the separation between foils) of the stack are determined, the following design was chosen with some considerations.
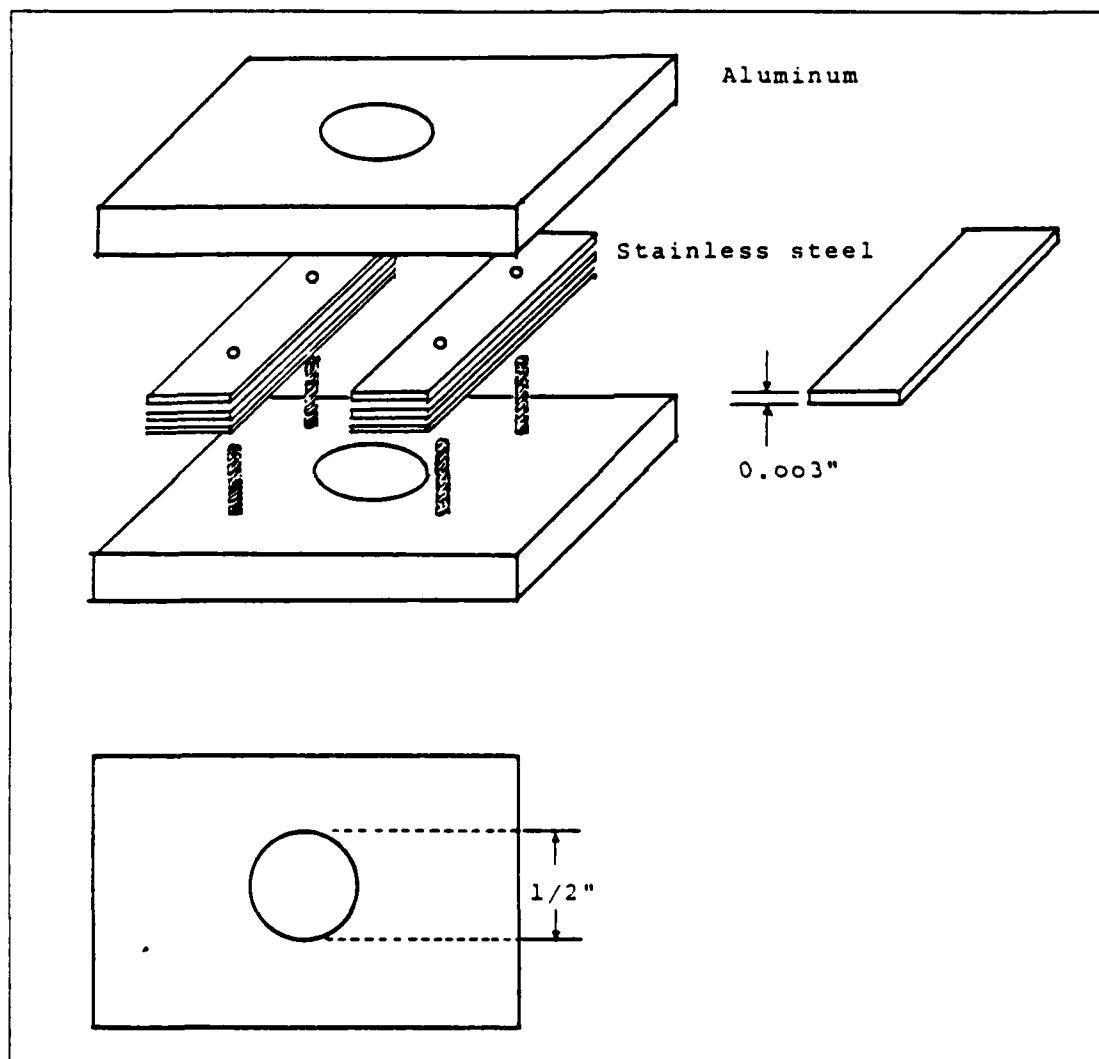
Figure D.1   Construction of stack.

The common difficulties which occur during the construction of stacks are in:

(1)   flattening the mylar without wrinkles which blocks the in-phase addition,

(2)   providing a ventillator for each spacing not to break out the mylar by the difference of the pressure between vacuum and spacing,

(3)   making all the spacing have the same separation to assure the coherent summation.

The construction of the stack in this experiment is sufficient to solve the two of three problems in above item (2) and (3), but the tension is not isotropic, it is in one direction, so few wrinkles can not be avoided.

LIST OF REFERENCES

1. Wartski, L., and others, "Interference Phenomenon in Optical Transition Radiation and its Application to Particle Beam Diagnostics and Multiple Scattering Measurements," *Journal of Applied Physics,* v. 46, No. 8, August 1975.

2. Frank, I. M., and others. "Radiation of A Uniformly Moving Electron due to Its Transition from A Medium into Another," *Journal of Physics,* v. 9, No. 5, 1945.

3. Ter-Mikaelian, M. L., *High-Energy Electromagnetic Processes in Condensed Media,* pp.194-376, Wiley-Interscience, 1972.

4. Garibyan, G. M., "Contribution to the Theory of Transition radiation," *Soviet Physics JEPT,* v. 6, No. 6, June 1958.

5. Cherry, M. L., and others, "Transition Radiation from Relativistic Electrons in Periodic Radiators," *Physics Review D,* v. 10, No. 11, 1 December 1974.

6. Piestrup, M. A., and others, *Detection of Coherent Transition Radiation and Its Application to Beam Diagnostics and Particle Identification,* paper presented at the U.S. Department of Energy, 13 January 1986.

7. Piestrup, M. A., and others, "Transition Radiation as a X-Ray Source," *IEEE,* v. QE-19, No. 12, December 1983.

8. Piestrup, M. A., and others, "Soft X-RAy Production from Transition Radiation Using Thin Foils," *Journal of Applied Physics,* v. 52, No. 1, January 1981.

9. Chu, A. N., and others, "Transition Radiation as a Source of X-rays," *Journal of Applied Physics,* v. 51, No. 3, March 1980.

10. Piestrup, M. A., and others, "Measurement of Transition Radiation from Medium-energy Electron," *Physical Review A,* v. 32, No. 2, August 1985.

INITIAL DISTRIBUTION LIST

No. Copies

1. Defense Technical Information Center
   Cameron Station
   Alexandria, Virginia 22304-6145   2

2. Library, Code 0142
   Naval Postgraduate School
   Monterey, California 93943-5002   2

3. Professor John R. Neighbours, Code 61nb
   Department of Physics
   Naval Postgraduate School
   Monterey, California 93943-5000   5

4. Professor Fred R. Buskirk, Code 61bs
   Department of Physics
   Naval Postgraduate School
   Monterey, California 93943-5000   5

5. Dr. M. A. Piestrup
   Adelphi Technology
   532 Emerson st.
   Palo Alto, California 94301   2

6. Yim, Chang-Ho
   160-01
   In-Cheon Si, Nam Gu, Seo-chang Dong, 170
   Seoul, Korea   10

7. Don Snyder, Code 61ds
   Department of Physics
   Naval Postgraduate School
   Monterey, California 93943-5000   1

8. Baek, Chil Ki
   SMC 1646
   Naval Postgraduate School
   Monterey, California 93943-5000   1

9. Jung, Yun Su
   SMC 2643
   Naval Postgraduate School
   Monterey, California 93943-5000   1

10. Hur, Soon Hae
    SMC 1645
    Naval Postgraduate School
    Monterey, California 93943-5000   1

11. Lee, Young Moon
    SMC 1110
    Naval Postgraduate School
    Monterey, California 93943-5000   1

END

4-87

DTIC